


8-2014

Self-Assembly of Gold Nanosphere Dimers by Inertial Force

George Andrew Christopher Sakhel
University of Arkansas, Fayetteville

Follow this and additional works at: <http://scholarworks.uark.edu/etd>

 Part of the [Biological Engineering Commons](#), [Inorganic Chemistry Commons](#), and the [Nanoscience and Nanotechnology Commons](#)

Recommended Citation

Sakhel, George Andrew Christopher, "Self-Assembly of Gold Nanosphere Dimers by Inertial Force" (2014). *Theses and Dissertations*. 2175.
<http://scholarworks.uark.edu/etd/2175>

This Thesis is brought to you for free and open access by ScholarWorks@UARK. It has been accepted for inclusion in Theses and Dissertations by an authorized administrator of ScholarWorks@UARK. For more information, please contact scholar@uark.edu, ccmiddle@uark.edu.

Self-Assembly of Gold Nanosphere Dimers by Inertial Force

Self-Assembly of Gold Nanosphere Dimers by Inertial Force

A thesis submitted in partial fulfillment
of the requirements for the degree of
Masters of Science in Biological Engineering

by

George Andrew Christopher Sakhel
University of Arkansas
Bachelor of Science in Biological Engineering, 2010

August 2014
University of Arkansas

This thesis is approved for recommendation to the Graduate Council.

Dr. Jin-Woo Kim
Thesis Director

Dr. David Zaharoff
Committee Member

Dr. Joshua Sakon
Committee Member

Dr. Matthew Patitz
Committee Member

Abstract

The morphology and composition of a nanoparticle (NP) play a critical role in determining the NP's properties and function. To date, researchers have created a myriad of NPs of different shapes, sizes, and compositions with interesting attributes and applications ushering a revolution in medicine, electronics, microscopy, and microfluidics.

In this study, gold (Au) nanosphere dimers (NSDs) have been synthesized through a novel self-assembly method. These particles were created from Au NPs mono-dispersed in aqueous solution via a process of centrifugation and capping agent replacement. Au NSDs consist of two Au NPs combined together with minimal gaps between them. Optical spectral analysis showed two wavelength bands: a wavelength band around 520 nm, which is attributed to the transverse surface plasmon resonance (SPR), and another wavelength in the near-infrared (NIR) region with a peak around 650 nm, which is attributed to the longitudinal SPR, as in the case of Au nanorods (GNRs). Synthesis of Au NSDs does not require toxic precursors, such as cetyltrimethylammonium bromide (CTAB) when making GNRs, suggesting that Au NSDs could be more clinically applicable nanotheranostic agents for molecular imaging and therapy as well as other applications such as drug delivery.

It is hypothesized that G-Force polarizes the NPs, which reduces the repulsive electrical double layer, allowing attractive van der Waal's forces to dominate and bring the surfaces in contact, causing surface reconstruction at the junction. The presence of capping agents, such as citrate, on the NP surface plays a key role in the electrostatic forces that bind the two spheres into a single, stabilized dimer by preventing further NP aggregation. Other popular NPs, including platinum (Pt) and silver (Ag) NPs were also investigated and showed significant shifts in SPR, suggesting that this method can be generalized across NPs of different compositions.

Although the detailed mechanisms and the applicability to other NPs with different shapes and/or compositions remain to be determined, considering its simplicity, controllability, and versatility, this G-Force driven technique could be implemented to assemble noble NP dimers with unique opto-electro-chemical properties for many applications, including optoelectronics, nanophotonics, biosensing, biosecurity, and nanomedicine.

Acknowledgements

I would first like to thank my mother, Sharyn, my father, George, and my grandparents, Mary, James, and Katy for being excellent role models and encouraging me to try new things and to further my education. Of course, without the advice and guidance of my advisor, Dr. Jin-Woo Kim, I would not have obtained the necessary lab or critical thinking skills required to complete a study of this magnitude. I'm grateful for Dr. Jin-Woo Kim's constructive criticisms as well as those of my committee members: Dr. Joshua Sakon, Dr. Matthew Patitz, and Dr. David Zaharoff who pressed me to improve the level of quality of my work. I would also like to thank Dr. Ji-Hoon Ya for teaching me the dimer formation process, Dr. Jeong-Hwan Kim for his work with the AFM, Dr. Mourad Benamara for his help and training with the TEM, Will Pierce and Stephen Grady for their help in the lab, Leanne Mathurin and Matthias Knust for their discussions on chemistry, Steven Dabic for his inspiration and conversations on physics, Bea Kachel for her help and loving support, Linda Pate for always being around to help me get through all the hurdles of graduate school, the great professors who taught my favorite classes, my lab-mates Joseph Batta, John Judkins, and Dr. Ki Taek Lim for helping me prepare my defense, my family for their continuous encouragement, and the UA Biological and Agricultural Engineering Department for financially assisting me during the majority of my research.

Contents

Chapter 1: Introduction	1
Chapter 2: Literature Review.....	5
2.1 Gold Nanoparticles	5
2.1.1 Gold Nanospheres	9
2.1.2 Gold nanorods	11
2.1.3 Gold Nanosphere Dimers	14
2.2 Surface Plasmons.....	16
2.2.1 Surface Plasmon Resonance	18
2.2.2 Controlling Surface Plasmon Resonance	20
2.2.3 Mathematical Modeling.....	21
2.2.4 Surface Plasmon Resonance Applications.....	22
2.3 Dimer Synthesis Mechanisms	27
2.3.1 G-Force, Weight by unit mass, inertial force.....	27
2.3.2 DLVO Theory	27
2.3.3 Surface Reconstruction.....	28
2.3.4 Casimir Force.....	30
2.3.5 Cold Welding	31
Chapter 3: Materials and Methods	32
3.1 Gold Nanoparticles.....	32
3.2 Silver Nanoparticles	32
3.3 Platinum Nanoparticles	33
3.4 Magnetic Nanoparticles.....	33
3.5 ATP-capped Gold Nanoparticles	34
3.6 Synthesis of Nanosphere Dimer.....	34
3.7 Imaging	37
3.8 Mathematical Model	38
Chapter 4: Results and Discussion.....	39
4.1 Image Analyses	51
4.2 Effect of G-Force.....	56
4.3 Generalization.....	63

4.4 Mechanism	72
Chapter 5: Conclusions	75
5.1 Future Recommendations.....	77
Works Cited.....	78
Appendix	89
1. DDSCAT Parameters.....	89

Chapter 1: Introduction

The morphology and composition of a NP play a critical role in determining the NP's properties and hence, function, driving much research to the development of procedures and synthesis of various NPs. [1, 2] Researchers have exploited this fundamental phenomenon and create a myriad of NPs of different shapes, sizes, and compositions with interesting attributes and applications ushering a revolution in medicine, electronics, microscopy, and microfluidics. [3, 4, 5, 6] Part of the reason that NPs have different behavior than their macroscopic counterparts is due to their colossal increase in surface area and the fact that they are small enough to exhibit quantum effects.

Particularly, Au NPs have shown characteristics such as low cellular toxicity and desirable optical, electrical, conductive properties which have driven its application for drug delivery [3, 7], electronics, and contrast agents. [8, 9, 10, 11, 4, 5, 6] Au NPs are finding themselves in more practical applications including drug delivery, electronics, microscopy, imaging, fluids, Microelectromechanical systems (MEMS), Surface Enhanced Raman Spectroscopy (SERS), and contrast agents. [3, 6, 7, 12] The topic of contrast agents and cancer therapeutics is of particular interest as it can be used to help improve the longevity and quality of human life.

An additional 1.6 million Americans are projected to be diagnosed with cancer and tumor related diseases this year. [13] There are numerous approaches to combat such diseases that range from preventative medicine, radiation treatments, surgery, and nanomedicine. Many contrast agents used in current approaches have negative toxic effects but various groups have shown that Au NPs in conjunction with photoacoustic imaging can provide excellent, noninvasive, *in vivo* imaging of cancer cells and can be applied for the detection of circulating tumor cells (CTCs). [8,

9, 14, 15, 16, 4, 17, 6, 18] Such detection could create a breakthrough in the early treatment and onset of metastatic tumors and has the potential to save many lives. Similarly, photothermal cancer treatments require NPs that resonate and heat upon application of an NIR laser which is safe to use on skin and tissue. [19, 20, 3, 6, 21, 16, 22] The therapy of photothermal techniques and the diagnostics of photoacoustic imaging can co-applied and is termed, *theranostics*. [3, 16, 17]

Gold nanorods (GNRs) have been used in NIR applications because they have a SPR in the NIR range which is a function of their composition, shape, and aspect ratio. Mie Theory gives the theoretical basis for the SPR of NPs and states that the color and hence absorbance of a very small particle is based on its optical resonance. [23] This was further expanded upon by Richard Gans that specifically, the aspect ratio of an object can be related to its absorbance peak and particles with a shorter aspect ratio tend to have absorbance lower on the electromagnetic spectrum than those with longer aspect ratio. [24]

Though GNRs are widely used for various applications in nanotechnology, their use in biomedical applications is impeded by their inherent toxicity as a result of the CTAB used in their synthesis. Their biocompatibility can be improved through ligand replacement, but this can create other issues such as complexity and incompatibility with bound therapeutic agents. Au NSDs overcome this limitation because their synthesis allows for further control and choice of capping agent, such as inert citrate as opposed to toxic CTAB. After centrifugation and capping agent removal, the two Au nanospheres self-assemble with minimal gaps between them. Optical spectral analysis showed results similar to GNRs of the same aspect ratio: a short wavelength band at about 520 nm, which is attributed to the transverse SPR, and a longer wavelength in the

NIR region with a peak at about 650 nm, which is attributed to the longitudinal SPR. [25] NSDs are formed without the need of additional chemical additives which is crucial for subsequent applications. [26] Additionally, the process for producing NSDs is simple, scalable, and cost-effective making it attractive for industrial manufacturing.

Au NSDs can be used as safe and effective near-infrared, plasmonic contrast agents for sensing, drug delivery, or theranostics. Furthermore, Au NSDs offer an alternative to GNRs particularly in biomedical treatments, diagnostics, and sensing applications because of their superior biocompatibility and simplicity. [16] The combination of inertial force, capping agent, electrostatic repulsion, steric hindrance, and gold's tendency towards surface reconstruction all play important roles in the mechanism by which two Au nanospheres combine to create a new nanostructure.

The mechanism behind the formation is hypothesized as the result of the dominance of attractive van der Waals over repulsive electrical double layer forces to allow the formation of Au NSDs. An applied G-force polarizes the NPs, which reduces the electrical double layer, allowing van der Waal's forces to dominate and bring the surfaces in contact which allows the NPs to undergo surface reconstruction at the junction. The presence of capping agents, such as citrate, on the NP surface play a key role in the electrostatic forces that bind the two spheres into a single, stabilized dimer by preventing further NP aggregation. Other popular NPs, including Pt and Ag NPs were also investigated and showed significant change in SPR, suggesting that this method can be generalized across NPs of different compositions.

The mechanism by which NSDs are synthesized may be important for the chemistry and physics and should be investigated. Electrostatic interactions, steric hindrance, surface reconstruction,

van der Waals, inertial force, entropy, and the Casimir Effect may all be factors in the fusion of two nanospheres. Additional investigation should be made to understand if the method itself is universal across different types of elements as this particularly can open the doors to other research and has important implications for the field of nanoscience.

In order to characterize NSDs and find hints towards their mechanism, Au NSDs must be synthesized through a trial of different parameters of G-Force, centrifugation time, volume, capping agent replacement, concentration, and procedure cycle repetitions. Further investigation using combinations of different sizes and compositions should also be explored. Transmission electron microscopy (TEM) at close range will be necessary to verify the crystal structure at the intersection of the NSDs and will be important in claiming a new shape has been physically formed.

Chapter 2: Literature Review

2.1 Gold Nanoparticles

Gold has been extensively studied on the nanoscale due to its conductivity, optical properties, and inertness in biological systems. [1, 3] Currently, scientists are able to create Au NPs in many shapes including spheres, ellipsoids, cubes, stars, triangles, bipyramids, nanoshells, and nanorods. [27, 28, 29] Different synthesis strategies are used for different shapes such as seeded growth techniques for nanorods, stars, bipyramids, and cubes [27, 30] or galvanic replacement reactions for Au nanocages. [30] Furthermore, Au NPs can be linked together by DNA to programmatically assemble nanostructures of increasing complexity. [31, 32, 2, 10, 33] Au NPs are an attractive subject of study because there are numerous methods for their synthesis, their surfaces are relatively easy to modify, and there are many tools available to detect and analyze them. [30, 32]

NPs can be controlled and altered using both Top-down and Bottom-up approaches. [34] Top-down approaches include electron-beam lithography, focused ion-beam, and optical lithography. These methods are advantageous for working in large areas, offer more precision, and can produce a wide variety of structures. Their limitations include slower speed and higher cost than Bottom-up methods. [34] Electron-beam lithography is commonly used to create nanosurfaces and nanostructures by emitting a beam of electrons at a film which may be used in etching.

Bottom-up, or “self-assembly”, approaches include deposition methods and chemical synthesis. These are more focused on the bulk control of NPs through chemical reactions that modify the properties of each particle. Bottom-up approaches are attractive due to their very low cost as well as the wide array of structures and shapes from which to choose. These approaches are still

lacking the control and precision that top-down methods are able to achieve, but this hurdle can be overcome as understanding of nanoscale phenomenon improves. [34]

Both Au and Ag NPs are popular noble metal NPs whose special morphology dependent properties are attracting researchers to exploit for imaging, photothermal theranostics, and label-free sensing. [35, 28, 21] Au is advantageous as it is chemically inert in many environments but is reactive to thiol-headgroup molecules, making it ideal for well-structured monolayers that can be built using groups such as alkyls, biomolecular groups, carboxylic acids, fluorescent dyes, and other organic molecules. [36, 31] These groups can attach to the Au surface by a sulfide bond and allow for greater control and tuning of the NP's properties. [36]

Au NPs can be functionalized by electrostatic or covalent binding of ligands, antibodies, or a variety of biomolecules as well ligand exchange reaction with thiols, phosphines, and surfactants. [1] These different functionalization methods can significantly affect the biocompatibility, surface charge, stability, and function of the Au NPs. The charge of the NP can also play a role in both its biocompatibility and function in a system. For example, significant changes in surface charge have been shown to influence the Au NP uptake rate possibly due to the NP's positive charge being attracted to the negative charge of the cell membranes. [37]

Applications

Au NPs are currently used and studied for applications including drug delivery [7], electronics, microscopy, imaging [12], fluids, MEMs, SERS, and contrast agents. [30, 6] Their wide spread use is due to their interesting electrical, conductive, and optical properties as well as their biocompatibility. [11]

Surface-Enhanced Raman Scattering (SERS) is a popular research area for noble metal NPs that is based on the theory that Raman signals can be amplified 10^9 to 10^{13} times simply as a result of extremely small inter-surface distance, creating an area known as a “hot spot”. [1, 38] This signal amplification could theoretically allow SERS applications and sensors to overcome current detection limits and reach single molecule sensitivity and detection. [39] Currently, SERS based biosensing can be used to detect proteins, ions, DNA hybridization, and other analytes without labels and without photobleaching as is common with fluorescent labels. [40] SERS research is continuously advancing but still struggles to produce quantitative detection and in synthesizing accurate and reproducible geometry to attain maximum field enhancements. [41]

The use of Au NPs for biological sensing or detection is limited in its specificity of binding, especially in the case of cancer detection where biomarkers are sometimes shared amongst different cell lines. A multiplexed detection method involving multiple target biomarkers can solve this limitation and allow detection of analytes in complex biological samples. [42, 14] Many researchers are attracted to NIR responsive Au NPs because of their application as smaller sensing probes that can additionally be used during surgery and endoscopy as well as when nuclear imaging is not an option. [43]

Recent research in the use of Au NPs as contrast agents has shown the potential they may have for the medical community. [9, 14, 15, 16, 6, 21, 22] Gold can be easily “tuned” as its optical properties are dependent on its size and shape. [44] This tunability is based on gold’s high electron density, intense light scattering, and absorption. Combined with gold’s low concentrations in the environment and biological systems, its properties make it an excellent nanomaterial for contrast agents. Various groups have shown that Au NPs in conjunction with

photoacoustic imaging can provide excellent, noninvasive, *in vivo* imaging of cancer cells and (CTCs). [8, 22, 3, 9, 17, 45] Such detection would create a breakthrough in the early treatment and onset of metastatic tumors and has the potential to save many lives.

CTCs are tumor cells that detach from a primary tumor site and circulate within the bloodstream, potentially causing metastasis in different tissues throughout the body. Although only about 0.01% of CTCs give rise to secondary tumors, metastasis resulting from CTCs is responsible for over 90% of cancer related deaths. [46, 47, 48] Removal or destruction of CTCs before metastasis can reduce and potentially prevent cancer from spreading in a patient's body. The detection of CTCs would reveal the potential locations of metastasis and as a result, enable physicians to monitor the growth of secondary tumors within these areas. Current methods of CTC include polymerase chain reaction (PCR), flow cytometry, and laser scanning cytometry. [49, 50, 6] These techniques are limited in their application because accuracy is dependent on the presence of CTCs within the particular blood sample. A typical blood sample is only 5-20 mL while the entire human blood volume is around 5 L; unfortunately, CTCs can be present anywhere within the bloodstream and may not necessarily appear in a given blood sample. [8] A way to overcome these obstacles is to identify CTCs within the entire bloodstream by use of functionalized Au NPs with photoacoustic flow cytometry *in vivo*. [8, 9, 14, 17, 45, 22]

A major component for photoacoustic flow cytometry is a durable, effective contrast agent. [6] Such a contrast agent must be able to produce a quality signal without harming the patient. In order to produce a signal, particles are immersed in laser light typically in the NIR range because it induces significantly less photodamage than lasers of other parts of the electromagnetic spectrum. As the NPs absorb the energy from the NIR laser, they can actually

lyse the cells in a similar treatment known as photothermal theranostics. [9, 17, 6, 21, 14, 18] *In vivo* photothermal theranostics are more attractive than chemotherapy because of their reduced toxicity and ability to image tumors in deep tissue, but are still limited by the lack of precise targeting of cancer cells. [45, 21]

2.1.1 Gold Nanospheres

Synthesis

Depending on their size, Au nanospheres have a single SPR in the range of 520-580 nm and can have diameters that range from 2 nm to over 100 nm. [29] Au nanospheres are commonly synthesized either through seeded growth or by the reduction of the metal salt HAuCl_4 in the presence of a capping agent, with the most common reducing agent being citrate. [30] Typical reduction methods are the Turkevich, Frens, and Prust preparations with Turkevich's method being the most popular since 1951. [30, 51, 29] The ratio of reducing agent to HAuCl_4 is important as the nanospheres' size varies with the amount of citrate; generally, larger NPs can be made by lowering the amount of reducing agent in relation to HAuCl_4 . [29] Although their study and use is popular, the exact growth, order of formation, and stabilizing mechanisms of Au NPs have yet to be clearly verified. [52]

Applications

Au nanospheres have seen frequent use in materials science and biomedical applications such as diagnostics, drug delivery, and sensing. [7, 3] The conductive and low resistance properties of Au nanospheres make them ideal for use in electronic circuits. Au nanospheres in aqueous solution can be "printed" onto plastic to make flexible and miniature electronics. [53] Some groups have used Au nanospheres as contrast agents to improve the signal of imaging techniques

such as photothermal interference contrast, dark-field imaging, reflectance imaging, and scanning electron microscopy. [29] Similarly, Au nanospheres can be used as contrast agents *in vivo* using photoacoustic flow cytometry and can detect circulating cells in real-time. [22]

Au nanospheres can be functionalized and “loaded” in order to facilitate specific binding or to carry a “payload” of drugs or molecules. [3] Anticancer drugs can be bound to polyethylene glycol (PEG) coated nanospheres which act as a transport vehicle to reduce systemic damage and allow more targeted treatments. One group attached tumor necrosis factor-alpha, which is systemically toxic, to Au nanospheres which were injected into mice with mammary carcinomas. They found significant tumor blood flow suppression when treated with a combination of the drug-loaded nanospheres and local heating which resulted in a tumor cell survival of 26% of the control value. [54] Cao et al. used Au nanospheres to detect prostate specific antigen (PSA) by measuring the Rayleigh light scattering of the Au NPs functionalized with PSA- α_1 -acntichymotrypson (PSA-ACT complex) monoclonal antibody. [55] Though the peak was not sharp, they achieved a peak shift of 2.85 nm and a detection limit reached 0.1 pg/mL. This research was improved by using GNRs whose local surface plasmon resonance (LSPR) is more responsive to adsorption than Au nanospheres. [55, 56] Similarly, Marinakos et al. created a simple, label free LSPR sensor in a chip-based format with nanospheres bound to a glass substrate to achieve a detection limit of 0.94 nM which they improved to 94 pM by exploiting the higher responsiveness of the LSPR of GNRs. [35]

2.1.2 Gold nanorods

Synthesis & Toxicity

GNRs have two plasmon bands: the transverse plasmon band which corresponds to its shorter axis is usually around 520 nm while the longitudinal band can have an absorption peak anywhere between 600-1800 nm, depending on the aspect ratio. [30] Though GNRs are commonly used in nanoscience, most preparations for GNRs require the use of CTAB which is toxic which presents complications in biocompatibility with living systems. [30] GNRs have a complicated synthesis and techniques vary, but the most common wet chemistry approach involves the anisotropic growth of the rods in a seed-mediated synthesis. [1] The seeds are small Au NPs in CTAB surfactant which is incubated in a growth solution containing ascorbic acid, gold salt, and silver ions. [57] The GNR particle size is controlled by the ratio of gold salt to seed concentration.

The toxicity of NPs is typically determined through *in vitro* experiments involving the incubation of cells with NPs. Once the toxic agent is found, strategies are employed to mitigate the toxic effects. These strategies can include over-coating the toxic agent, zipping the agent to the NP, or replacing the agent with a more biocompatible molecule. [1] Over-coating with polyelectrolytes decreases the toxicity of CTAB by lowering its desorption from the Au NP. Zipping involves more permanently attaching the toxic agent to the Au NP by polymerization. With CTAB, for example, a polymerizable version of CTAB can be polymerized on the Au NP which was shown to significantly increase the biocompatibility due to the decreased CTAB desorption. [1]

Replacement of toxic surface chemicals after the GNR has formed is also a promising strategy for reducing cytotoxicity. Since complete removal of CTAB will result in GNR aggregation, researchers use a variety of different substitutes to replace CTAB and make the GNR more

biocompatible. [55] Methods for the replacement of CTAB include CTAB extraction with an organic solvent followed by capping with less toxic ligands, cationic exchange for CTAB molecules through competing ligands, displacing with thiols, or incubating with thiolated PEG which have all shown to decrease toxicity of GNRs significantly. [1]

The type of ligand functionalized on the GNR can affect the cellular uptake rate. A study using particles of aspect ratios 1.5 to 4.0 and the ligands CTAB, sodium polyacrylate (PAA), and polyallylamine hydrochloride (PAH) showed PAH to be taken up by the cells the fastest (2000 PAH-GNR/cell vs. 250 PAA-GNR/cell vs. 50 CTAB-GNR/cell). [1] The ligand plays a major role in determining biocompatibility. CTAB-GNRs were shown to reduce cell viability to 30% while PAA-GNRs and PAH-GNRs were nontoxic at the same concentration of 0.4 nM. [1] The cytotoxicity of CTAB-GNRs was shown to be independent of surface charge as both anionic and cationic CTAB-GNRs had similar toxicity profiles. [1]

GNRs are more difficult to functionalize than Au nanospheres because of the presence of the strongly binding CTAB. This bond can lead to aggregation of GNRs and therefore drastically affect its optical and electrical properties. Another shortcoming of CTAB synthesized GNRs is poor stability in bases, organic solvents, or in the presence of low CTAB concentrations. Many groups have come up with strategies to combat this, but it generally comes at some cost such as increased hydrodynamic size or increased aggregation. [1]

Applications

Since 2001, GNRs have been widely used in nanotechnology for applications ranging from MEMS, imaging, electronics, SERS, and biological applications. [1, 35] Part of their widespread use is due to their high aspect ratio which results in unique electrical and optical properties. This

morphology explains why GNRs absorb wavelengths of light ranging from visible to the NIR (600 nm -1100 nm) depending on the aspect ratio. [1] The longitudinal peak is of particular interest because it is very sensitive to changes in medium and environment and it can be “tuned” by changing the length. [58] The sensitivity to the medium is also distance dependent meaning that the binding or localizing of analytes can be qualitatively detected. [35] These properties of tuning and sensitivity make GNRs better candidates for SPR based sensing than Au nanospheres. [35] NP absorption in the NIR range is important for biomedical applications because these wavelengths allow for imaging of deep tissue with minor damage. The SPR of GNRs allows them to be used in the body and ‘activated’ by an NIR laser for detection of cancer, proteins, and other targets of interest within a living body. [8]

Researchers have taken advantage of the sensitivity of the optical absorbance, efficient light scattering, and physical properties of GNRs to develop methods for sensing and detection. GNRs can be synthesized so that their longitudinal surface plasmon resonance (LSPR) will be accurate within 1 nm absorption. [1] This precision can be exploited to obtain a qualitative analysis of adsorption of a target analyte in biological or other systems. One of the lowest detection limits of 111 aM was recorded by a Troung et al. who were able to get an absorbance shift of 2.79 nm in a label-free bioassay for PSA in phosphate buffer saline solution. [55] Also remarkable was their apparent use of single nanorods as detection sensors which they achieved by replacing the CTAB coating with $\text{HS}(\text{CH}_2)_{11}(\text{OCH}_2\text{CH}_2)_6\text{OCH}_2\text{COOH}(\text{OEG}_6)$ which allows for stronger bioconjugation of the prostate-specific antigen. Single GNR sensors were realized as a result of molecular binding at and near the GNR surface which can significantly change the refractive index of the medium surrounding the NPs corresponding to a LSPR shift. [55]

The SERS enhancement for GNRs is seen in a variety of different applications ranging from detection of cancer [58] and prions in biological media [41, 39] or tagged *in vivo* sensing. [42, 40, 20, 15] The *in vivo* applications are particularly interesting for GNRs because their optical properties work greatest in the NIR which is safe for biological tissues. [43] Detection methods and sensors using GNRs are being improved by reducing steric hindrance that prevents analyte adsorption and optimizing the precision of morphology of the GNRs to reduce noisy data. [56] Though GNRs can be exploited for their LSPR sensitivity, this technique is not limited to GNRs and it has been done with other Au NPs of different shapes such as nanospheres, bipyramids, and triangles. [27, 35, 28]

2.1.3 Gold Nanosphere Dimers

An alternative to GNRs are Au nanosphere dimers which are made up of two joined Au nanospheres. The names dimer, binary NP, snowman-shaped NP, or dumbbell have been used throughout literature to refer to a NP made up of two nanospheres. Dimers are particularly sought after for use in SERS because of their strong theoretical electromagnetic field enhancement which may allow single particle applications. [59] The area between the two particles, the junction, is predicted to be a “hot spot” with particular field enhancements; however, touching particles give a lesser field enhancement than particles separated by a very small distance. [59]

Most existing dimers or dumbbells are bound together by a linker and synthesized using DNA, crystal substrate [60], molecule, ligand [11], or solid phase approaches. [61, 62] The disadvantage of the DNA linker is the need to use electrophoresis to remove excess product, though this does result in a high yield of dimers and allows for the ability to exploit DNA's

programmability for further control and assembly. [10] Au NPs of different sizes can be used and various non-rigid orientations created depending on the DNA binding strategy. [63] Brousseau et al. used Phenylacetylene oligomers as a linker between Au NPs because of its rigidity, conductivity, and the ability to control its length and binding angle. [11] They were able to produce both dimer and trimer Au NP structures.

Solid phase approaches, in which the reactions are conducted on a solid support such as a polymer resin, can also produce dimers of different compositions, but again, require the use of a chemical linker. [64] Sardar et al used a chemical linker to create dumbbells through a modified solid phase approach that could allow for wide range of sizes. [62] Starting material of citrate Au was prepared by the Turkevich method and then immobilized on a silanized glass substrate. After 2 hours incubation with 1mM 11-mercapto-1-undecanol (MUOH) in ethanol, a monolayer of thiol molecules self-assembled on the outer surface of the NPs. The NP bound plates were then sonicated in 16-mercaptohexadecanoic acid (MHA) which then asymmetrically bound to the glass side of the NPs when they dissociated from the glass plate. The purpose of this process was to create the first half of the dimer. The second half of the dimer followed the same procedure except with mercaptomethylamine (MEA) instead of MHA. To connect the two pieces, the MHA functionalized NPs were reacted with 1-ethyl-3-(3-dimethylaminopropyl)carbodiimide hydrochloride and 1-pentafluorophenol for 2 hours before finally combining with the MEA functionalized NPs and stirred for 4 hours at room temperature resulting in a dimer. An additional benefit of this procedure is the ability to change the distance between the two spheres by varying the length of the linker molecules. [62]

Au dimers are similar to GNRs in that their aspect ratio can result in absorbance in the NIR range, indicating possible use in biological systems. However, Au dimers are quite different from GNRs in many ways. Most obviously, the shape looks more like the combination of two spheres than a single rod. Experiments by Tchegotareva et al. showed that the dimer shape had an additional characteristic acoustic wave that was due the combination of particles. [65] Roca et al. produced dimers and trimers of silica gold NPs via centrifugation and without additional chemical components. This simplicity is important for NP purification and subsequent application, particularly for biological systems. [26] Surely, there will be more properties directly the result of the dimer shape as further research is pursued.

2.2 Surface Plasmons

Since 1992 there has been a considerable increase in scientific papers using the terms surface plasmons, signifying their importance and broad application throughout science. [66] Surface plasmons are exploited in many areas of science ranging from optics, chemistry, electronics, and biology. Surface plasmons are the clouds of free conducting electrons at the surface of metals that react to heat, electricity, and light among other phenomena. [67]

Surface plasmons exist in metals because metals have free conduction electrons. These electrons are by definition a 'plasma' because they are a neutral 'gas' of electrons. These plasmas are neutral because the negative charges are balanced by the fixed positive ions of the metal. [66] Surface plasmons are a kind of solid-state plasma, which is where the word plasmon and the field of plasmonics has its root. [66]

Free conduction electrons play a huge role in the properties of metals; they are the reason metals have 'good' optical properties the same way they have 'good' thermal and electrical conductivity

properties. [66] This plasma of free conduction electrons controls the optical properties of the metal and thus the plasma's reaction to light will describe a particular metal's reaction to the same light. It is commonly known that metals have 'good' optical properties in the visible wavelength range because they act as mirrors and reflect light well. The mechanism that explains these 'good' optical properties is a result of metals having a resonant wavelength that exists in the visible range, depending upon the particular metal.

Surface plasmons at the interface of two materials can be thought as "propagating electron density waves occurring at the interface between metal and dielectric." [68] Surface plasmons are especially strong if one of the materials is a metal as it provides free electrons because of metal's abundance of free electrons. The electrons act as waves that stay within a short boundary creating a strong field at the interface.

There are multiple types of surface plasmons, two of which are Surface Plasmon-polaritons at planar interfaces and Localized Surface Plasmons-polaritons. [66] Surface Plasmon-polaritons are used in wave propagation and sensing applications. Localized Surface Plasmon-polaritons play a major role in electromagnetic field enhancements and SERS. [38]

Modeling of surface plasmons and SPR is difficult because modeling of ions, electrons, and quantum phenomena is necessary. Studying light at the nanometer scale is also difficult because the diffraction limit prevents optical resolution of NPs smaller than several hundred nanometers. [34] Exciting phenomena occur when a NP or material is equal to or smaller than the diffraction limit and was first explored by Michael Faraday in the 1800's. [69] Surface plasmons provide a means by which light can be used to detect events at the nanoscale or even enhance electric

fields. Field enhancement of metal NPs occurs in the visible light spectrum where their surface plasmons have a resonant frequency. [70, 71]

2.2.1 Surface Plasmon Resonance

Electrons act as a cloud that responds to an electric field. They respond by moving to one side of a particle and when they move in tune with the electric field, there is a resonance called a SPR. Particle shape or surface is important because it takes a different amount of time for the electrons to move depending on the shape. There are also effects from coupling and from the area around the particle of interest such as pH, pressure, and electric as well as other properties. Particle properties that are particularly important are size, shape, sharp or curved edge, and dielectric constant. [70]

When light hits a metal NP, the free conducting electrons will oscillate with the electric field. They move away due to the force caused by the incident light but will return towards the NP because of the Coulomb attraction between the electrons and the nuclei of the NP. [72] This oscillation frequency is determined by the electron density and mass, and shape and size of the charge distribution.

SPR can also be defined as the oscillation of free conduction electrons driven by incident light and can be likened to a mechanical oscillator. [69] At a particular resonant frequency, this oscillator will achieve its maximum amplitude and will absorb the maximum amount of incident light. Light shown onto an object will reflect a different percentage of light based upon the angle of incidence. [68] At a certain angle, surface plasmons begin to excite until SPR occurs when the intensity of reflected light is at a minimum. This angle is called the SPR angle and is

dependent upon optical, morphological, and electrical characteristics of the object and its surroundings.

Refraction is important in SPR as it affects the SPR angle. The refractive index can be used in determining adsorption onto an object in sensing applications because the refraction will change proportionally with the change in adsorption. Therefore, the change in adsorption can be measured by a shift in the SPR angle. This can be useful for determining biomolecule adsorption kinetics and is attractive because it is label-free, meaning it does not use an isotope to label the particle/molecule under investigation.

In the special case where two NPs are separated by 1 nm to 2 nm, SPR can provide electric field enhancements up to 10^{11} due to an increase in absorbed energy; this provides the fundamental basis for SERS. [38] Such enhancements will be observed within a local area known as the evanescent field whose calculation explains some properties at the interface. [68] The evanescent field is relatively small and decays exponentially with distance from the surface plasmons. [73]

Just as there are different plasmons, there are also different modes of plasmon resonance that can occur. Dipole modes that act along an axis are commonly studied with regards to nanospheres. [72] Quadrupole modes can occur where half of the electrons move perpendicular to the applied electric field. Multipole modes can be reached through precision and control of the properties that affect surface plasmons. The multi-disciplinary efforts in surface chemistry, optics, and microfluidics helped establish today's conventional SPR understanding, sensors, and instruments. [68, 71]

2.2.2 Controlling Surface Plasmon Resonance

There are many controllable factors that will affect the SPR for NPs which include size, shape, surface roughness, local surroundings, and the composition of the material. NPs greater than 10 nm have a SPR that is dramatically affected by the size. As a particle size increases, its resonant wavelength also increases and there is an increase in the amount of absorption and scattering.

The particular absorption and scattering both contribute to optical extinction of a NP. [34] LSPR can be “tuned” by adjusting particle size, for example, increasing size from 10 to 90 nm could result in a SPR wavelength shift from 520 to 560 nm. [34]

Shapes of NPs have incredible variety ranging from ellipsoids, rods, stars, crescents, voids, sphere, dimers, cages, core/shell structures, toroids, to disks. Shapes with sharp features tend to have better field enhancement and core/shell structures such as nanocages as well as toroids have also shown strong SPR. Aspect ratio is especially important and shapes such as rods and disks have a SPR peak that corresponds to their major longitudinal axis and another peak corresponding to the minor transverse axis. [73]

SPR is in a sense, the a study of a local area, and the area surrounding the particle or surface chemistry will also cause effects such changes in refraction. A surrounding dielectric material, for example, can affect the dispersion and confinements of the surface plasmons. [73] The composition and surface roughness of the material affects SPR particularly if larger than 10 nm and different metals will have different SPR even if they are the same size. [74] For example, Ag NPs have a more localized wave propagation mode but have a lesser red-shift than Au NPs. [73]

In addition to these single particle properties there is also an entire field, SERS, dedicated to taking advantage of the SPR and electric field enhancements that exist between two NPs and nanostructures separated by a distance on the order of 10-50 nm. [38] The size of this gap is similar to the decay length of the electromagnetic field associated with the surface plasmon mode. [66] SERS research shows that theoretically the nanosized gaps between NPs will lead to strong electromagnetic field enhancements. [38, 71]

2.2.3 Mathematical Modeling

Mathematical modeling of a phenomenon such as SPR is complex. A vast amount of non-trivial variables exist as well as their multifaceted interactions. These variables include interactions of electrons with ions, impurities, phonons, as well as other quantum phenomena. Each of these variables is difficult to treat by their own right; the amalgamation of them all creates a daunting task for computation. [66]

Many models such as Mie Theory, Drude model, the finite difference time domain [74], T-matrix methods, and the Discrete Dipole Approximation (DDA) are used in the field of plasmonics. [59] Mie theory is concerned with the scattering properties of a sphere and can be understood as: Extinction = Scattering + Absorption. [72] It was devised by Gustav Mie in 1908 and is an exact solution to Maxwell's equations that describe extinction spectra for spherical particles. [66] Its advantage is that it is one of the few exact solutions available but comes at the cost of serious complexity in calculation and can only be applied to spheres and infinite cylinders.

Originally published in 1973, the DDA was intended for astrophysics but over time has become popular for use in plasmonics, nanotechnology, and SERS. [75, 66, 76] DDA is a powerful

method for the study of individual NPs that treats a single NP as a cubic array made up of N polarizable spheres. [59] Under an electric field, each sphere will have an induced dipole which will in turn create an electric field and induce the dipole of every other sphere in the lattice. The induced dipole moment at each of these cubes is solved exactly and related by the Clausius-Mossotti relation to the overall NP in order to approximate the absorption and scattering efficiencies for the overall NP. The Clausius-Mossotti equation relates the microscopic polarizability to the macroscopic response:

$$\epsilon - 1 = \left[\frac{4\pi N\alpha}{1 - \left(\frac{4\pi}{3}\right) N\alpha} \right]$$

where ϵ is the bulk dielectric constant, α the complex polarizability, and N the number of atoms in unit volume. [66, 75] This breaking up into a cubic array allows the DDA to be used for arbitrary shapes other than the spheres required by Mie Theory. [76] DDA is advantageous in that it is conceptually simple and does not discretize the surrounding medium. However, the amount of computing power necessary can be heavily dependent on the choice of shape. [66] Another significant disadvantage is that the choice of number of dipoles can heavily affect the outcome of results, making the DDA better for approximating populations of NPs rather than close study of an individual NP. [77]

2.2.4 Surface Plasmon Resonance Applications

SPR has been exploited to monitor molecular adsorption, protein-protein interactions, and other biological reactions in real time. [78, 79] Since changes in refraction causes shifts in angle, one can record the SPR angle to monitor changes with the biological adsorption. The area of significance around the sensor is limited to a couple hundred nanometers, within the range of the

evanescent field. The field strength decays exponentially with distance from the sensor which is encouraging in terms of signal interpretation if the sensor can get close to the target. In order to have accurate targeting, the sensor needs to be specifically functionalized so as to have affinity for the target and not the surrounding materials.

Surface chemistry plays an important role in SPR-based biosensors because a ligand needs to securely bind to the metal surface. Hydrogels, highly absorbent networks of hydrophilic polymer chains, can be attached to thiols which can be bound to a Au surface. These hydrogels can facilitate biomolecular binding due to their high absorbance and they are thin enough to stay within the 200 nm evanescent field past which the SPR effect is significantly diminished. [68]

The first SPR sensors were created by Lundstrom in 1983 during which he measured the properties of molecules using ellipsometry, refractometry, SPR, photothermic detection and other methods. Around the same time, researchers at the University of Twente were investigating transduction principles and successfully demonstrated measurements of immunochemical reactions using SPR. Au became the metal of choice for biosensors because it is more inert than Ag and therefore more suitable for biological applications even though Ag typically has a larger SPR effect. [66]

Since 1990, Biocore has been the leading company in SPR instruments, being cited in 87% of biosensor-related publications. [68] Carboxymethylated dextran has become a common surface due to its biocompatibility and excellent immobilization of biomolecules. [68]

Improvements in SPR sensor design and data analysis have led to a 20-fold increase in SPR sensor sensitivity and 100-fold increase in data range. [68]

A SPR assay mainly consists of an analyte and ligand, which is specially chosen to remain bound to the metal surface while also being attractive for the analyte. It is crucial that the bond between the ligand and metal remains strong throughout the entire procedure else adsorption cannot be easily quantified. Once the ligand is secured to the metal surface, the analyte is injected. In direct detection experiments, there will be a shift in SPR angle over time as the analyte binds to the ligand in the association stage. In general, unwanted components in the injected solution may also bind to the ligand but this is remedied by injection of a proper buffer solution that will remove unwanted binding without influencing the ligand or the analyte. The dissociation of the analyte to the ligand can then be studied without interference. Finally, addition of a “regenerative” solution will remove the analyte without affecting the ligand’s bond with the metal surface to allow for additional reuse of the sensor. [68] This process of analyte injection, purifying, and cleaning is repeated with the same ligand-metal complex in order to obtain accurate measurements on kinetic and thermodynamic processes of interest, particularly biological processes.

Small particles and low concentrations of NPs cause difficulty and unreliable data in SPR measurements, therefore small particles or molecules need to have a large number of bindings in order to produce a significant signal. Similarly, low concentrations of a target analyte are difficult to distinguish and therefore SPR measurements have a minimum threshold that must be met. [68] Furthermore, there is a finite amount of binding sites which creates a detection ceiling as there can only be as many bindings as there are binding sites. In general, absolute measurements are not crucial and simply the change in refractive index is sufficient.

The kinetics in SPR measurements can be studied through the calculation of association and dissociation rate constants as well as their equilibrium constants. Association is described by the reaction of $A+B \rightarrow AB$ while dissociation is described by $AB \rightarrow A+B$. Association equilibrium constants, K_A , are calculated by $[AB] / [A][B]$, where a high K_A value indicates a high affinity for binding. The dissociation equilibrium constant, K_D , is calculated by $[A][B] / [AB]$, where a high K_D corresponds to low stability of binding. [68]

A typical SPR instrumentation set-up will include an optical unit, liquid handling unit, and sensor surface. [68] The optical unit can be a prism or glass, grating, or a type of optical waveguide. The liquid handling unit allows for solution to be controllably injected and removed. The sensor sits between the optical and liquid sections and plays the vital role of exhibiting plasmon resonance and ligand binding.

A recent example of surface plasmons in the biomedical and biosensing field can be found in the research of Robelek et al from 2012. [80] The group focused on using SPR based instruments to monitor the volume changes of cells and cellular structures. Volume changes within cells can be linked to different physiological and pathophysiological events occurring in the cell and understanding these events can help in characterizing certain diseases, cellular response, and cell function in general. Current methods for monitoring cells in real-time have a variety of limitations ranging from high interference and limited sensitivity, to photobleaching and phototoxicity effects caused by labels or contrast agents. [80]

The SPR of metals are responsible for the enhanced electromagnetic field that occurs in SERS and intensities in Raman scattering vary with the integral of the local electromagnetic field to the fourth power depending on the particular nano-geometry. [74] One research group in Germany

uses the special properties of surface plasmons for the fabrication of a nano-optical antenna. [81]
The antenna is based similarly to SERS, using the gap between two NPs to change the resonant frequency. Since plasmons are so sensitive, even a minor change in gap distance will change the resonant frequency. [71]

Surface plasmons play a wide and important role in the field of nanoscience. From their origin in optics, to their use in photovoltaic devices, biosensing, and microscopy, surface plasmons are indeed essential in many nanoscale studies. While still limited in our techniques for physical manipulation and detection as well as more precise mathematical modeling, progress in plasmonics is steadily being made.

2.3 Dimer Synthesis Mechanisms

The exact mechanism by which NSDs form is uncertain though it may be due to the combination of G-Force, van der Waals, and electrostatic forces. Derjaguin, Landau, Verwey, and Overbeek (DLVO) theory and surface reconstruction may also help in describing the mechanism. Finally, fusion of two nanospheres may also be a result of the quantum effects of the Casimir force or cold welding.

2.3.1 G-Force, Weight by unit mass, inertial force

Researchers have used mechanical force to create and physically alter NPs, including nanowire and Au dimers. [82, 26] Roca et al. hypothesized that the electrical double layer surrounding the Au NPs is polarized when under G-Force which attracts and binds the NPs together. [26] Au NPs in solution experience an electrostatic repulsion, but can experience electrostatic attractions when polarized under G-Force. [26] The group found that optical properties and geometric alignment of NPs are dependent on the magnitude of G-Force as well as the removal of the citrate buffer. [26] Binding occurs when the electrical double-layer is compressed, decreasing its repulsion, and van der Waals forces become the dominant force. Van der Waals forces are inherent to the NP and inversely proportional to the sixth power of their separation. [83] Both the electrostatic repulsion and van der Waals forces are inversely proportional to the interparticle distance making G-Force an important parameter for their control. [83]

2.3.2 DLVO Theory

The electric double layer is the electric potential of the NP. [83] Widely used in colloidal science, DLVO theory relates the attractive van der Waals forces to the repulsive forces of electric double layer. Between two surfaces, a lowering of the electric double layer will result in

a net attraction and the total interaction can be described as sum of van der Waal's attraction and electrostatic repulsion. [82] As the two NPs are pushed close together, eventually their electric double layers will overlap, resulting in a repulsion which has a maximum based on the double layer thickness. At a certain distance very close, the repulsion reduces dramatically and van der Waals forces dominate, causing the two NPs to attract and combine. Slightly further away is the maximum repulsive force produced by the electrostatic double layer so as the double-layer is compressed, repulsion increases until the critical point where the forces between the particles become attractive and the particles instantly combine. [83]

Stability of the NP is a function of the solution conductivity, Brownian motion, surface chemistry, and the balance of electrostatic repulsion with van der Waals forces. [26] The surrounding medium is particularly important as it influences the magnitude of van der Waals and electrostatic forces surrounding the NPs, allowing for aggregation or binding. [26] Further aggregation is prevented by electrostatic repulsions and the steric barrier of the capping agent. [83, 84] In particular, citrate Au NPs are electrostatically stable due to the citrate trianions adsorbed on their surface. [84]

2.3.3 Surface Reconstruction

Due to intermolecular forces, atoms within a crystal will align themselves in a period structure. However, there is a difference between the atoms within the bulk material and the atoms at the surface, since the surface only experiences the intermolecular forces from one direction, which results in a significant decrease in electron density at the surface. [85] This results in the surface atoms having an altered structure or position referred to as either a relaxation or a reconstruction. For most metals, the surface layer will contract slightly or shift in order to minimize potential

energy. For 5d metals (Ir, Pt, Au) surface interactions or adsorption onto a surface can commonly cause a surface reconstruction in which one or more layers change their two-dimensional structure as well as position in order to minimize stress or energy. [61]

Surface reconstruction can either be conservative or non-conservative, where the number of atoms on a layer is more or less than before reconstruction began. The tendency of a metal surface to undergo reconstruction is based on numerous factors such as surface energy, surface stress, and interatomic force constants, many of which can be currently estimated experimentally using Scanning Tunneling Microscopy (STM) or computationally with density functional theory. [85, 86, 61] The exact mechanism for surface reconstruction is still incomplete but Mansfield and Needs have devised the theory commonly cited by researchers. [86] Their theory states that surface stress is the driving force for the reconstruction, balanced by the amount of energy required to bring an extra atom onto the surface layer and the energy change brought onto the surface atoms. [61]

Au surfaces have a tendency to reconstruct and have been calculated to have bond-lengths approximately 10% shorter [86], and the energy of a surface atom is about 10 meV higher than that of the ideal bulk material. [85] Additionally, research has shown that a curved gold surface in contact with another gold surface will prefer to be flat rather than curved. [36] The curves will be “filled in” during rapid surface restructuring which may occur due to the reduction of the Laplace pressure which reduces the free energy of a molecule at a curved surface. [87] Further study into surface reconstruction is useful not only for our understanding of the physical phenomenon and self-assembly, but also for applications in advanced circuits and optoelectronic devices. [88]

2.3.4 Casimir Force

The Casimir effect or Casimir-Polder force is the physical attractive force of two electrically neutral objects with nanometer separations that is a result of fluctuations in zero point energy in an electromagnetic field and can be described by quantum field theory. [89] When two conducting parallel plates are very close (for example, 10 nm), vacuum electromagnetic energy density in between the plates will be less than outside, resulting in an attractive pressure. [90]

The force is nonlinear and increases rapidly at distances less than 500 nm. [91] This results in a net attraction because there are less electromagnetic modes between the plates. Making two plates extremely parallel (10^5 rad for 1 cm plates) is very difficult in practice, so it has been common to measure the Casimir effect between a flat plate and sphere, avoiding the issue of parallelism to experimentally validate the theory. [91] Recently, an international group overcame the issue of parallelism through electron-beam lithography and achieved separations of 70 μm . [92]

The Casimir and van der Waals forces are related, but the Casimir force can be attractive or repelling depending on the geometry as theorized by Lifshitz. [93] For example, two plates will attract, while two hemispheres of a split sphere will repel; additionally, two bodies in liquid medium can be either repulsive or attractive. [91, 94] Some groups want to harness this repulsive force for use in MEMS or Nanoelectromechanical systems (NEMS), circuits, sensors, or for extremely low-friction devices. [90, 92, 95] The Casimir effect is one of the many interesting quantum phenomenon that we see at the nanoscale.

2.3.5 Cold Welding

Some groups have reported the phenomenon of “cold-welding”, “capillary wetting”, or “sintering” of NPs which results in the merging of two metal NPs under low loads and without the need for heating. [96, 97, 87, 98, 36] The process occurs when NPs are pressed together or come in contact with their capping agent removed. The combination of the NPs occurs abruptly when a critical pressure or interparticle separation is reached. [87, 36] When the atoms of two similar metal NPs are in contact, there is no way for the atoms to “know” which NP they are a part of. [99] Alcantar et al. found the “jump-in” point to be 10 nm, concluding that a mechanism or force other than just van der Waals must also be taking place in order to be attractive at that distance. [87] Similarly, Knarr et al. found the “jump-in” point to be at about 25 angstroms. [36] Both research teams found that the two Au surfaces had indeed become one and, afterwards, proceeded to pull the two surfaces apart. Again, both groups reported the same interesting finding: the Au surfaces didn’t break at the newly formed interface but, instead, the Au broke from its mica substrate and remained bound to the other Au surface.

The materials do not necessarily have to be the same composition as Au NPs have been stably “welded” to Ag NPs without detectable alloying. [96] Interestingly, it was also found that when different metals such as Ag and Au were cold-welded together, the Ag NPs seemed to behave as a soft material that “wets” a Au NP. Additionally, the detrimental effect of “dirt” or organic layers is significantly lower than expected. [87, 98] As our know-how continues along with our ability to fabricate and manipulate structures at the nanoscale, improvements to health, industry, and everyday life will become obvious.

Chapter 3: Materials and Methods

3.1 Gold Nanoparticles

Au NPs were created by the combination of HAuCl_4 and Sodium Citrate Dihydrate (Sigma Aldrich) by the Turkevich method as per the procedure described by McFarland et al. [100] Wavelength absorbance was tested using a DU 800 ultraviolet/visible/NIR spectrophotometer (Beckman Coulter Inc., Fullerton, CA) or a NanoDrop 2000c Spectrophotometer software version: 1.4.2 (Thermo Scientific). Optical spectra were normalized to the maximum absorbance except when noted otherwise. The size of the Au NPs and NSDs were verified using transmission electron microscopy. Citrate was added in different amounts to obtain different sized Au NPs. The sample tubes used were the economy micro tubes with snap caps and 1.5 mL volume (VWR). The distilled water (ddH₂O) used was purified using the EASYpure® RF system (Barnstead, Dubuque, IA; 17.8 Ω). Regents were purchased from VWR (West Chester, PA) or Sigma-Aldrich (Milwaukee, WI) except for HAuCl_4 which was bought from Strem Chemicals (Newburyport, MA). Centrifugation was performed using Microfuge® 18 Centrifuge with F241.5P rotor (Beckman Coulter), the long term centrifugations by the Biofuge pico (Heraeus), and the high G-Force centrifugation by an Avanti™ J-25 Centrifuge with rotor JA-25.50 (Beckman Coulter). Au NSDs were made with 0.00010545 g metal/mL solution.

3.2 Silver Nanoparticles

NPs of different elements were synthesized in order to investigate the potential of the NSD technique to be generalized across different compositions. Ag NPs were synthesized following the procedure used in Ratyakshi et al. [101] 0.18g AgNO_3 (Amrexco, Solon, OH) per liter ddH₂O was reduced by a 1% Sodium Citrate (Sigma) solution at 1 mL Sodium Citrate solution

for every 10 mL AgNO₃ solution. Mixture was boiled at 120°C until it turned a pale yellow color. [101] During the NSD procedure, higher volumes were spun down to appropriate concentrations before diluting with water. Ag NSDs were spun down at 13,000 RPM for 30 minutes prior to dilution and processing. Ag NSDs were made with 0.00010391 g metal/mL solution.

3.3 Platinum Nanoparticles

The approximately 30 nm Pt NPs were synthesized with Platinum Chloride reduced by methanol purchased from (Strem Chemicals). [102, 103] 3 mL of methanol was heated to 70°C in a 3-neck round bottom flask connected to a reflux condenser and stirred at 1000 RPM. The methanol was cleaned with nitrogen gas for 2 minutes to make it inert. 0.82g of 0.1 M PtCl₆²⁻ was diluted into 20 mL ddH₂O and 0.1 M disodium citrate was diluted into 60 mL of ddH₂O. 1 mL of the PtCl₆²⁻ solution was added by syringe into the heated methanol. After 10 minutes, the citrate solution was added drop-wise and the total mixture was heated for another 15 minutes as the color changed from yellow to brown to black. The final concentrated solution showed an absorbance peak around the 230 nm wavelength. Pt NSDs were made with 0.00010549 g metal/mL starting solution and the results shown used a 4X solution.

3.4 Magnetic Nanoparticles

30 nm spherical magnetic iron oxide NPs (MNPs) were purchased from Ocean Nanotech (Springdale, AR). MNPs exhibited the strongest absorption at short visible wavelengths. [14] Magnetic NSDs were made with 0.000105263 g metal/mL MNP solution.

3.5 ATP-capped Gold Nanoparticles

The capping of adenosine triphosphate (ATP) on Au NPs was prepared by mixing 1 mg/mL of Au NPs in ddH₂O with 0.6 mM ATP ligands at 25 °C for 6 h. The dissociated citrate and free ATP were easily separated by addition of pyridine (20 mL), followed by a rotary evaporator-based drying. After removal of the pyridine layer, the precipitated Au NP layer was washed with pyridine two times and thoroughly evaporated. Finally, the dried dark Au NP product was redispersed into 1 mL of water.

3.6 Synthesis of Nanosphere Dimer

Au NSDs were created from Au nanospheres capped with citrate. At room temperature, 100 μ L of Au colloid NPs are combined with 100 μ L of ddH₂O in a 1.5 mL sample tube. The sample tube was centrifuged at 13,000 RPM (15587.72 x g) for 10 minutes until aggregate formed at the bottom. Afterwards, the supernatant was carefully removed without disturbing the aggregated NPs and replaced by an equivalent volume of ddH₂O. Optimal removal will decrease the amount of procedure cycles needed, but over-removal will dilute the results. After light vortexing and centrifugation, the sample was sonicated in a Model 75T Sonicator (VWR) until the pellet of NPs at the bottom separated into the solution. The UV/Vis absorption spectra were taken between 400 and 800 nm on a spectrophotometer using 70 μ L UV-Cuvette micro 12.5x12.5x45 mm and center height 8.5 mm (Brand, Germany). This process is termed a “cycle” and cycles were repeated 3 times with the capping agent removal step; afterwards, the sample undergoes the same centrifugation process, but no more capping agent is replaced because its effect has weakened due to minimal residual capping agent. The process is continued without capping

agent removal until there is a significant color change from red to blue. An overview of the NSD procedure is shown in Figure 1.

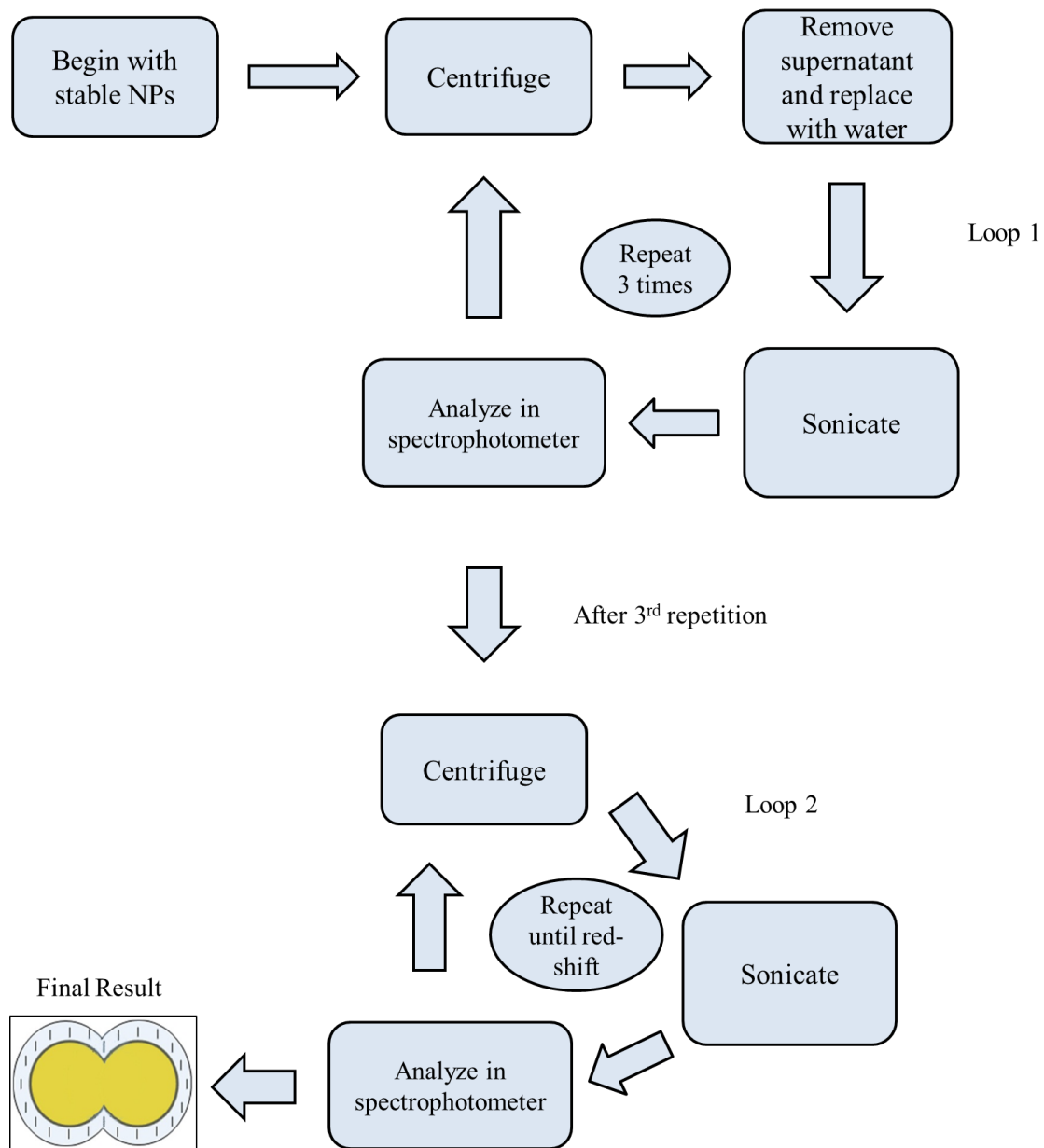


Figure 1. Overview of NSD synthesis.

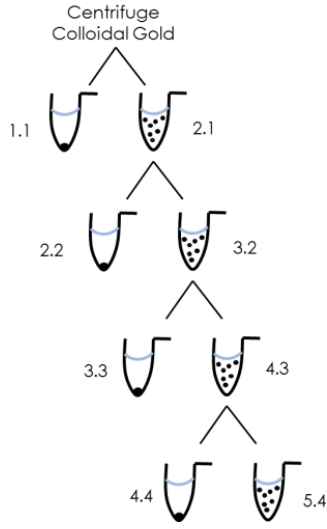


Figure 2. Separation outline.

In order to obtain a higher yield, a modified NSD procedure was designed using centrifugation methods. Figure 2 shows the separation outline. A sample of colloidal gold was centrifuged at 13,000 RPM for 10 minutes as before. Afterwards, however, the sample was lightly vortexed with a Vortex-genie 2 (Scientific Industries) at 9 intensity with the idea being that the large particles (the NSDs) are tightly packed and stuck against the wall, while the smaller particles (the Au nanospheres) are lightly aggregated. All solution was removed and placed into a new sample tube labeled 2.1 as seen in Figure 2. The tube with the aggregated NPs and without any solution was then filled with 100 μL of ddH₂O and scanned in the spectrophotometer. Tube 2.1 now becomes the starting material for the next separation loop and the process continues as shown in Figure 1. Generally, tube 1.1 does not have any Au NPs in it because the NSDs have not yet formed. The majority of NSDs are found in sample 3.3 which is unsurprising as this is the equivalent centrifugation cycle that NSDs are seen in the NSD procedure without separation. Samples 2.1, 3.2, 4.3, and 5.4 tend to show a much larger peak at 522 nm than 645 nm, confirming assumptions that the Au nanospheres will float in free solution upon light vortexing.

3.7 Imaging

Transmission electron microscopy (TEM) and atomic force microscopy (AFM) were used in order to obtain a visual image of the NP shape and size. The particles for TEM were prepared by the NSD procedure and 2 μL of NSDs were diluted with 8 μL of ddH₂O to decrease aggregation and imaged with an FEI Titan 80-300 S/TEM operating at 300kV and fitted with a CEOS image

corrector. Images show the NSD separation procedure at 5X dilution. 2 μL of the unstained, diluted sample was pipetted onto a 300 mesh carbon-coated copper grid and allowed to air dry before being examined using a JEOL 100CX electron microscope (JEOL-USA, Peabody, MA). [18]

AFM samples were imaged with a Veeco Multimode Scanning Probe Microscope with Nanoscope IIIa Controller (Veeco Instruments, Woodbury, NY). Similarly to the TEM preparation, for AFM analysis, 2 μL of NSDs were diluted with 8 μL of ddH₂O and 2 μL of the mixture was placed onto a mica substrate (Novascan, Ames, IA) and allowed to dry. AFM samples used the tapping mode with a NanoWorld Pointprobe® NCSTR AFM probe (Nanoworld AG, Neuchatel, Switzerland). This probe is designed to give extra stability and accuracy during soft tapping mode imaging in order to produce higher quality AFM images while minimizing sample damage. [31] The sample scan rate was 1.0 Hz with an aspect ratio of 1:1 and the free resonance frequency of the cantilever was automatically tuned by the Nanoscope Software (version v5.30r3sr3; Veeco Instruments) as suggested by other research. [31]

3.8 Mathematical Model

The freely available DDA program, DDSCAT, was run for single sphere and two spheres in contact with the full parameters file in Appendix 1. [104, 105, 106] The program was run to compare 14 nm diameter Au NPs in a dielectric environment of 1.333 and the refractive index for Au was taken from the work by Johnson and Christy. [107] Absorbance between 400 and 800 nm were calculated with dipoles on the order of 10^6 as suggested by Crow. [76] The single sphere was modeled using the function “ELLIPSOID” and the dimer was modeled using the function “SPHROID_2.” [104]

Chapter 4: Results and Discussion

To verify the creation of a new particle, absorbance and size tests were performed. Absorbance of NSDs was tested against a control group of Au nanospheres and showed a significant absorbance peak at 648 nm. Figure 3 shows the absorbance comparison of Au nanospheres versus the NSDs.

The absorption of NSDs can be seen by the purple line in Figure 3. This is a dramatic change from the starting material shown by the blue line. There was no change in the NP solution until the 2nd cycle (green) which produced a slight shift beyond 600 nm. On the 3rd cycle (purple), a secondary peak formed and the maximum SPR has red-shifted from 522 nm to about 648 nm. There is still a strong peak at 522 nm indicating that a portion of Au nanospheres still exist in solution. In line with previous research on GNRs [26], the 522 nm peak of the NSDs is also due to the transverse axis while the 648 nm is due to the longitudinal axis. As previously discussed, it is known that a change in surface plasmon resonance can be the result of a change in shape. [108] More specifically, Mie theory predicts this secondary peak to be the result of a change of aspect ratio. The prominent SPR peak shift gives an experimental basis for the hypothesized change in shape from Au nanospheres to NSDs.

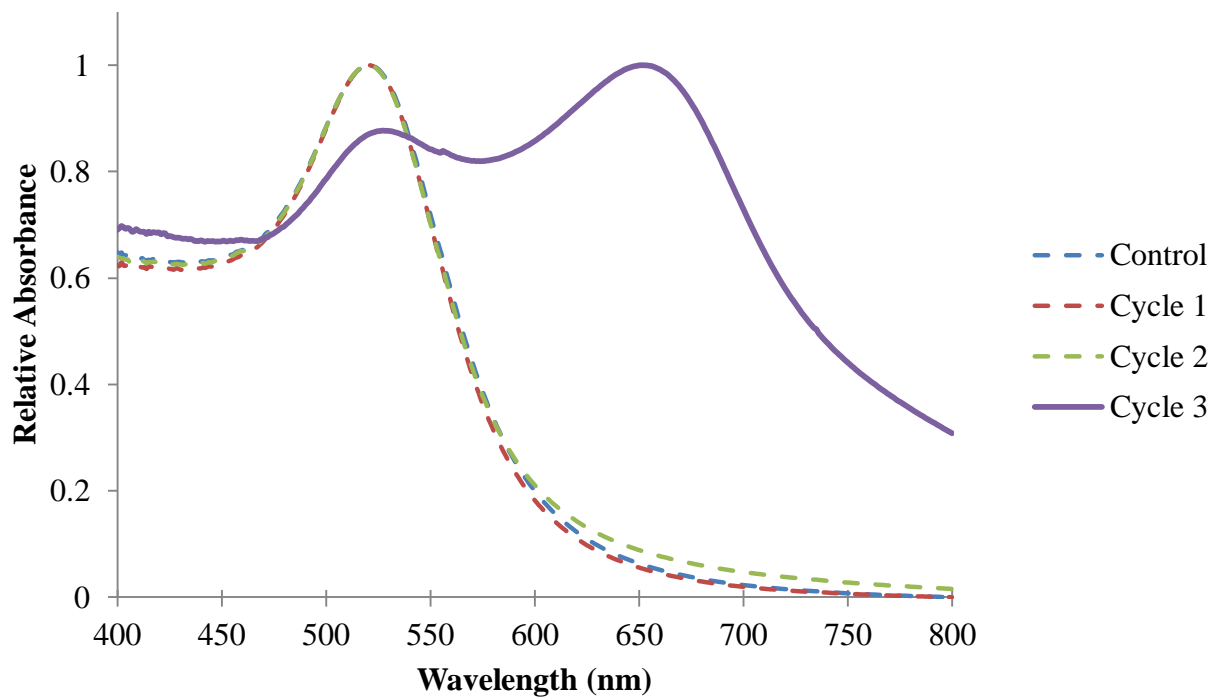


Figure 3. Absorbance Spectra of NSDs.

To test whether NSDs can be created in a higher yield, the samples were separated by centrifugation. The UV/Vis Spec results in Figure 4 show a higher percent yield of NSDs (red) in a separation by centrifugation procedure as compared to NSDs created without the separation procedure (purple). The lower Au peak at 522 nm relative to its 648 nm peak indicates that there is a lower percentage of spheres in the separated NSD sample when compared to the unseparated NSDs. The green line shows the absorbance of the solution that was removed from the NSDs. It has a much lower absorbance peak at 648 nm and a raised peak at 522 nm, indicating that this removed solution contains a majority of free floating, unbound Au nanospheres. This ability to separate and purify is important for scaling up and for industrial application where sample purity is necessary.

As seen in Figure 5, after the 1st centrifuge, spherical NPs aggregate together at the bottom and are surrounded by a red halo at the tip of the test tube. The red is indicative of Au nanospheres with a SPR peak around 522 nm. As the NSD synthesis procedure continues, the solution becomes blue with a SPR peak around 648 nm and the centrifuged sample no longer shows the red halo around the pellet.

The effect of repetitions can be seen in Figure 6 where there is a dramatic increase in the maximum wavelength on the third cycle. Afterwards, there is no significant change in peak absorption wavelength and any variation can likely be attributed to experimental error. From the raw data, there seems to be an optimal amount of cycles after which there is a decrease in absorbance intensity simply due to losses during the procedure.

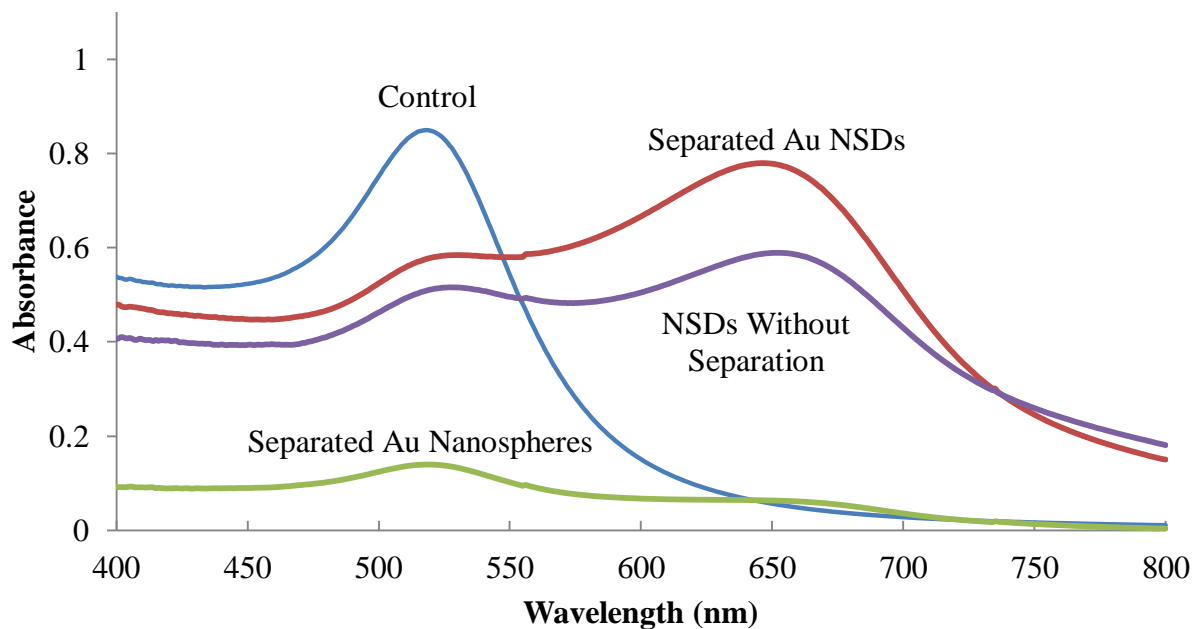


Figure 4. Absorption of NSDs without separation by centrifugation compared to NSDs synthesized with centrifugation separation.

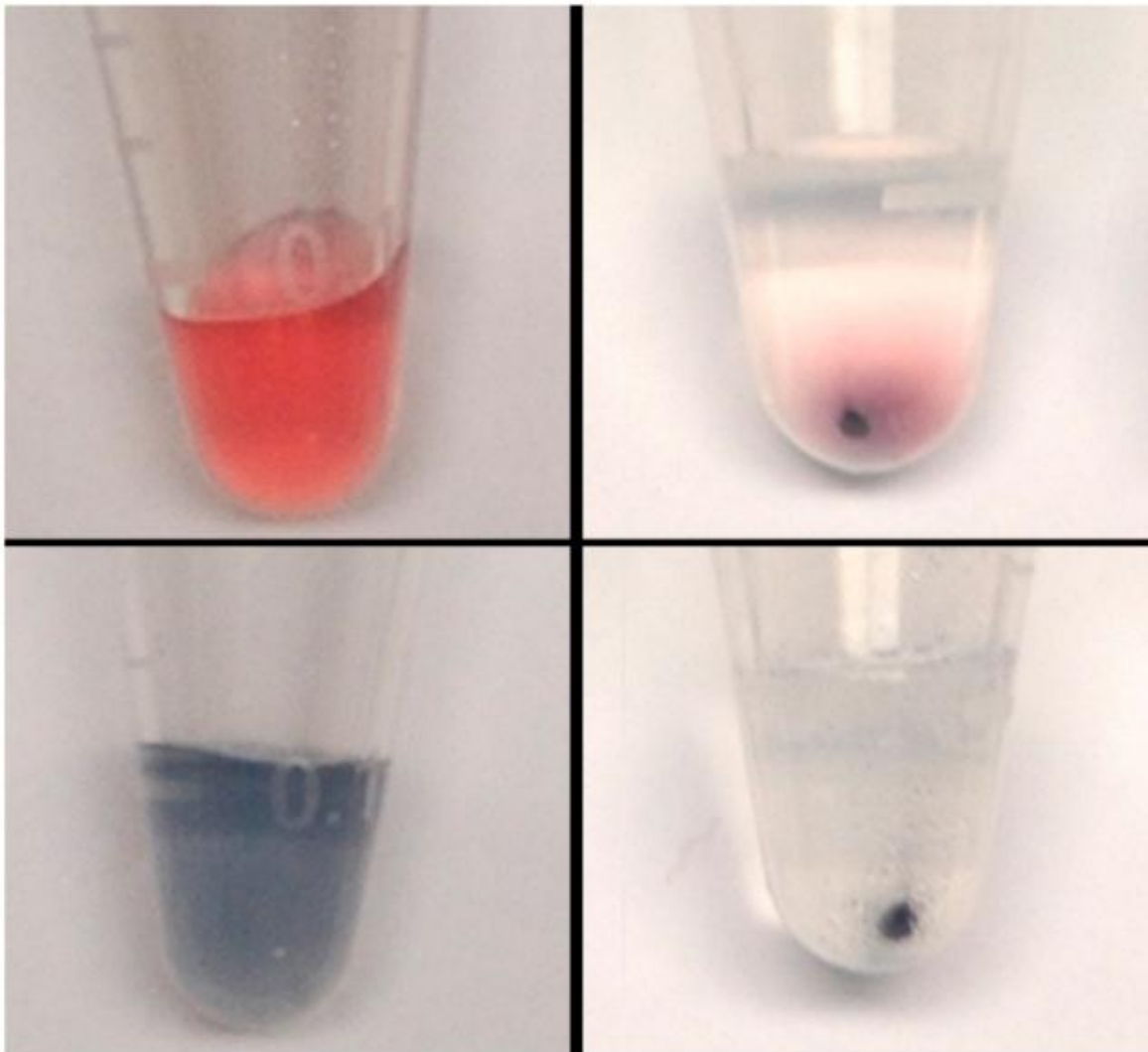


Figure 5. The visual change from nanospheres to NSDs. The topleft picture shows the starting Au solution, topright shows solution after 1 centrifugation. Bottom left picture is the NSD solution, and bottom right is the centrifuged NSD solution.

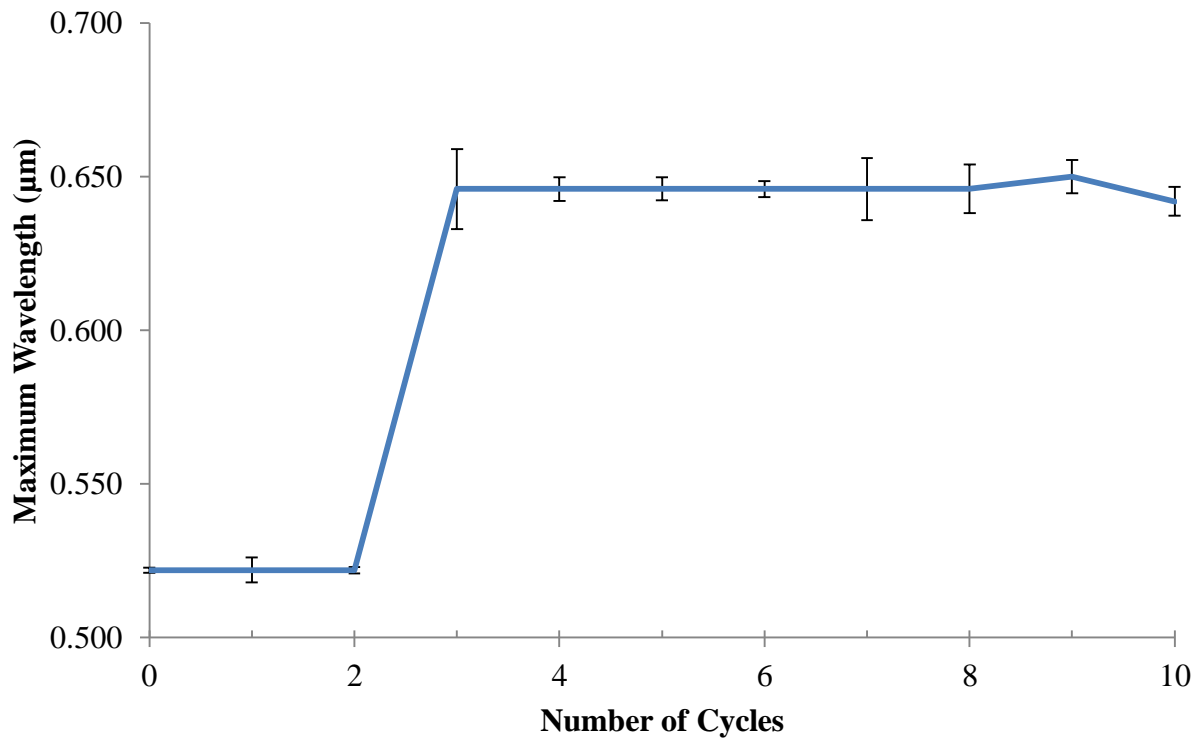


Figure 6. The peak absorption wavelength of NSDs using different number of cycles

Figure 7 shows the comparison of the NSD procedure ran with a capping agent removal step versus no capping agent removal. Removal of the capping agent, in this case citrate, produces much less variation and is quite consistent when compared to the NSD procedure ran without citrate removal. Without capping agent removal, the NSD procedure appears to only cause minor aggregation which is indicated by the slight widening of the base of the UV-Vis Spec curve. From this we can conclude that a capping agent removal step is necessary for the creation of NSDs if the rest of the procedure is to remain constant. Citrate creates a negatively charged medium for the NSDs and it appears that the removal of its excess from the citrate capped Au NPs has a significant effect on the synthesis of the NSDs. Additionally, the charge of the medium versus the charge of the NPs may have important consequences for the mechanism by which the NSDs form.

The role of charge and capping agent can also be seen in Figure 8 where previously created NSDs were combined with the same citrate capped Au NPs used in their synthesis. The starting NSDs (red) show the expected 648 nm peak and the starting citrate Au (blue) show the 522 nm peak. Interestingly, when the two are combined (green), the 648 nm peak significantly reduces. It appears that the excess citrate breaks up the NSDs back into single spheres, however, there still exists an absorbance shift beyond 550 nm. This is likely due to the NSDs disassociating imperfectly, resulting in non-spherical shapes. Importantly, the NSDs can still be recreated by continuing with the procedure and it again takes 3 cycles to obtain NSDs (orange). The recreated NSDs in orange have a blue-shifted peak compared to the original NSDs in red which may be due to the non-spherical, heterogeneous NPs, created from the disassociation step, merging together. This significant finding suggests that the NSD procedure is both controllable and tunable.

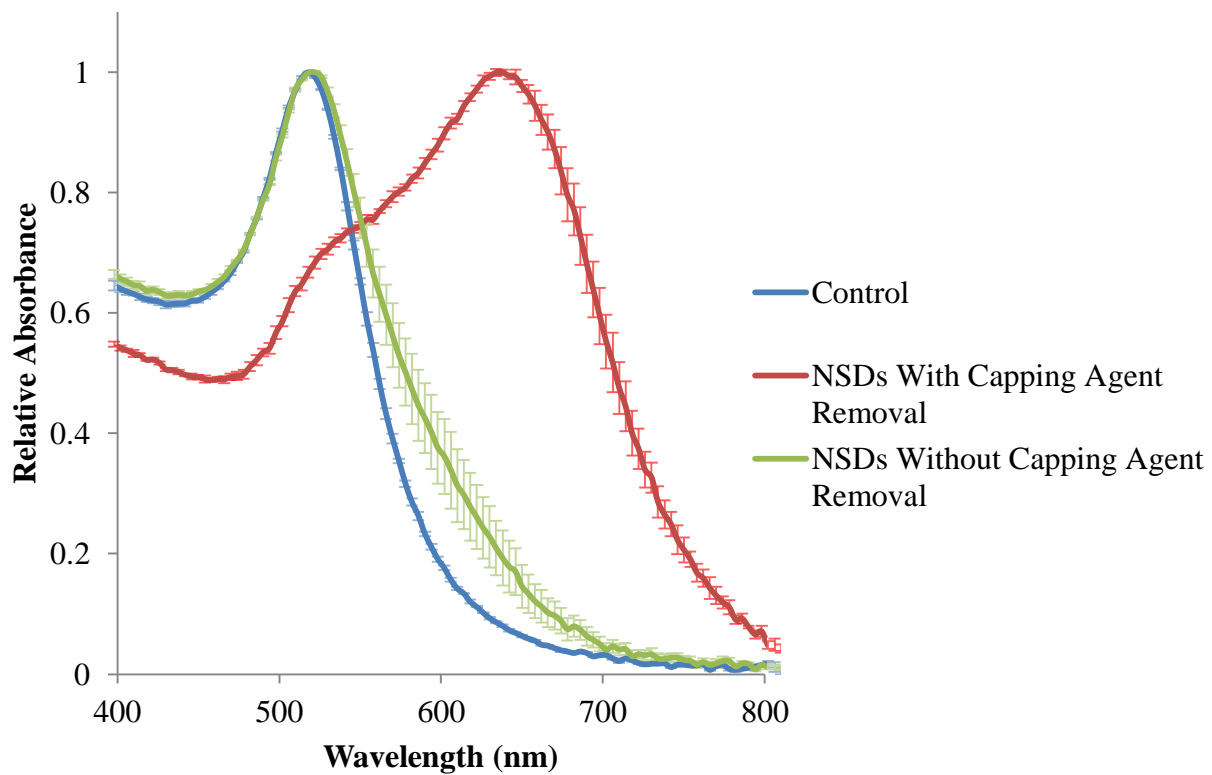


Figure 7. The NSD synthesis using capping agent removal (red) compared to NSD synthesis without the capping agent exchange (green).

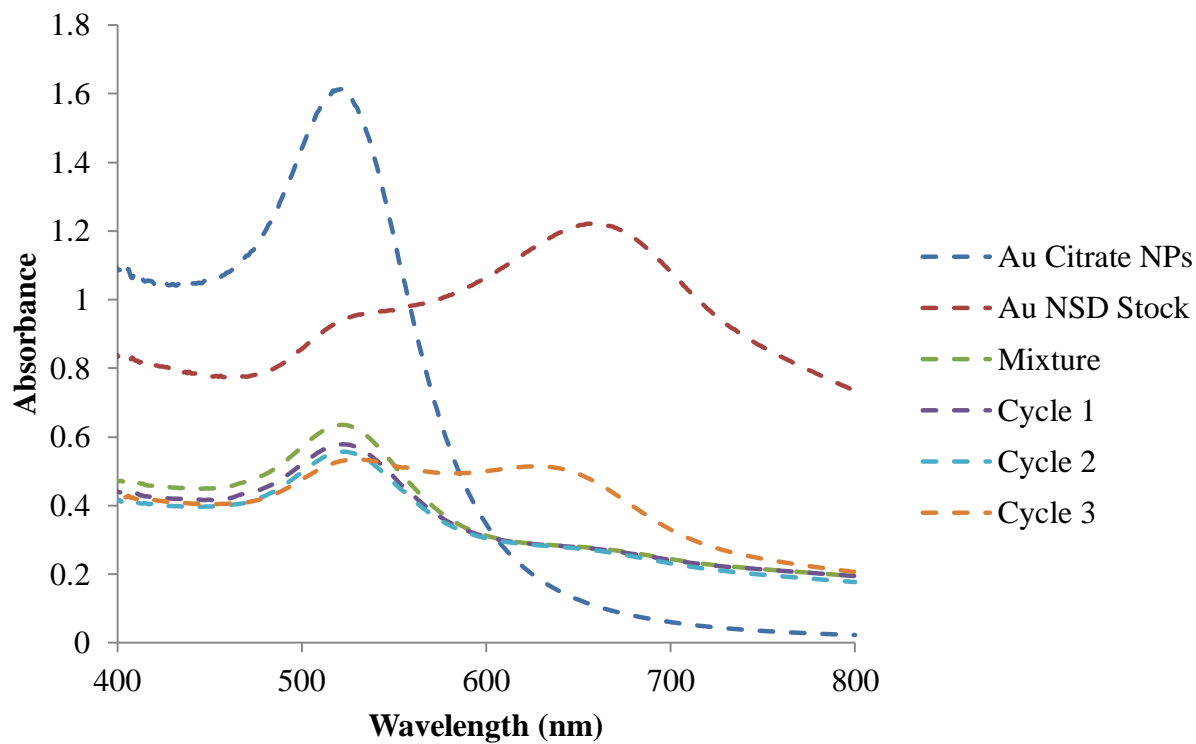


Figure 8. NSDs mixed with equal parts Au Citrate NPs.

Figure 9 shows separated Au NSDs (blue) were recombined with separated nanospheres (red). Their mixture (green) shows both the 522 nm and 648 nm peaks and indicates that no shape change occurred upon mixing. There is not a disassociation of NSDs as seen in Figure 8 because there is not an excess of citrate as both solutions of Au nanospheres and NSDs were diluted in ddH₂O. Therefore, the higher 522 nm peak relative to the 648 nm peak in the mixture is simply the result of additional Au nanospheres present in solution. Running the mixture through the NSD procedure produced an expected but slight increase in the purity of NSDs seen as the purple line in Figure 9.

All experiments used 1.5 mL eppendorf tubes except for those used in Figure 10 which used a smaller 0.5 mL tube in order to explore the effect of the smaller tube tip where the NPs will aggregate. The results in Figure 10 look similar to Figure 3: cycle 1 shows no shift, cycle 2 shows a slight shift, and cycle 3 shows a dramatic peak increase. However, the NSD peak in Figure 10 (purple) is closer to 670 nm than 650 nm indicating that the space available for NP binding has an effect on the final NSD formation. This, again, is important as it allows for simple tuning of the NSDs.

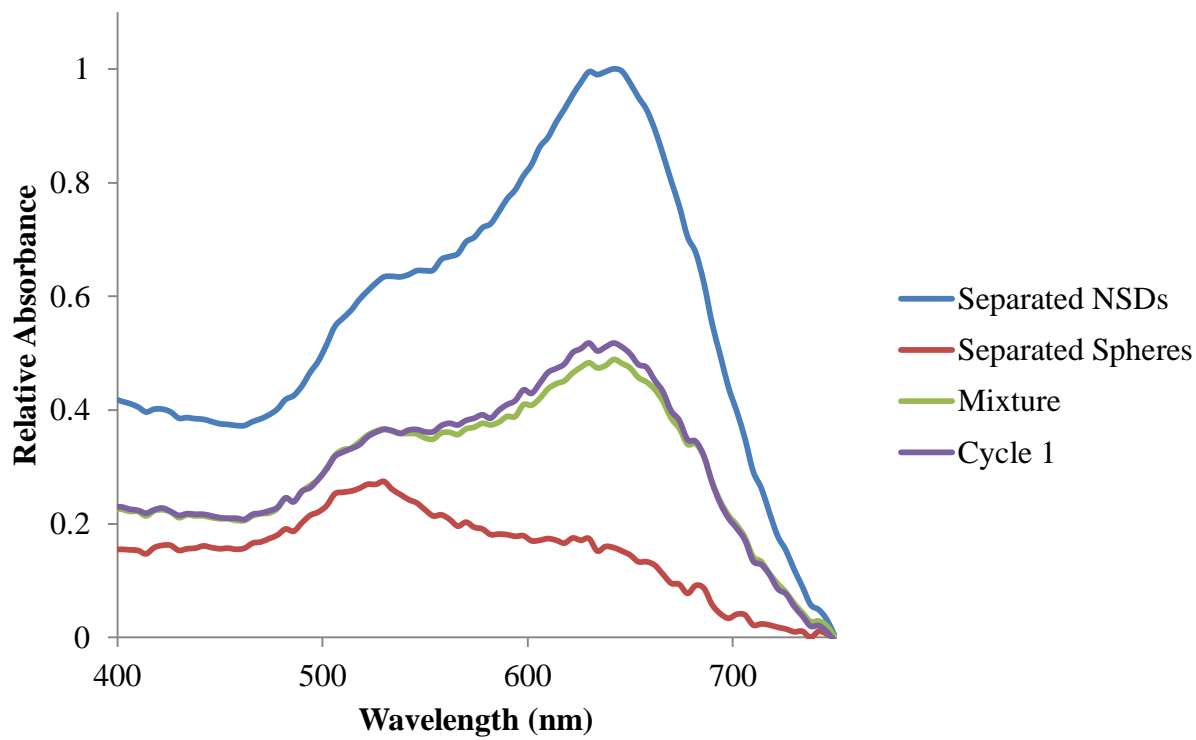


Figure 9. Separated NSDs mixed with Separated Au Nanospheres.

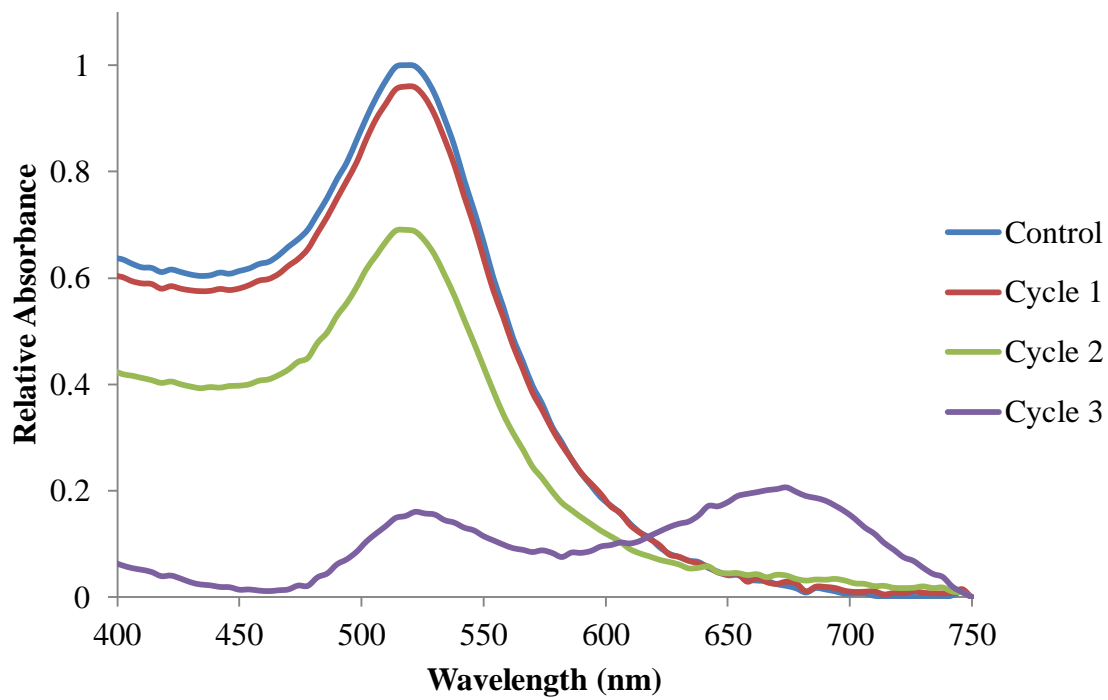


Figure 10. NSDs created with a smaller sample tube.

4.1 Image Analyses

In order to verify the shape predicted from the absorbance results, TEM and AFM analysis were performed. Figure 11a shows the TEM image of the starting citrate capped Au nanospheres. The Au NPs tend to aggregate and line up when drying the sample for TEM, but there is still a clear separation between the lined up NPs. This is in contrast to Figure 11b where there seems to be at least two spheres combined into a single particle which is then grouped with others. From TEM measurements, it was confirmed that Au NSDs were created from starting material of 14 nm citrate capped Au NPs which in turn produced 28 nm Au NSDs. Figure 11c shows a zoomed-in look at the connection between the two spheres from a high-resolution TEM image of the isolated NSD shown in the inset. The crystal lattice of the Au NSD appears to connect from one sphere to the next, indicating that the NSD is in fact a single particle which is in agreement with the shape predicted from Mie Theory.

The TEM image in Figure 11b seems to show NSDs, but it is difficult to distinguish. Part of the reason for this is the attractive properties of the Au NPs during sample preparation. As the sample is dried, the Au NPs aggregate together, creating difficulty in discerning whether single particles are lying together or whether two spheres have fused together. This self-assembly during drying is characteristic for particles at the nanoscale and is also seen in the drying of nanorods. [1] This may be improved upon through the use of flash drying techniques or the addition of a buffer solution to keep the particles separate.

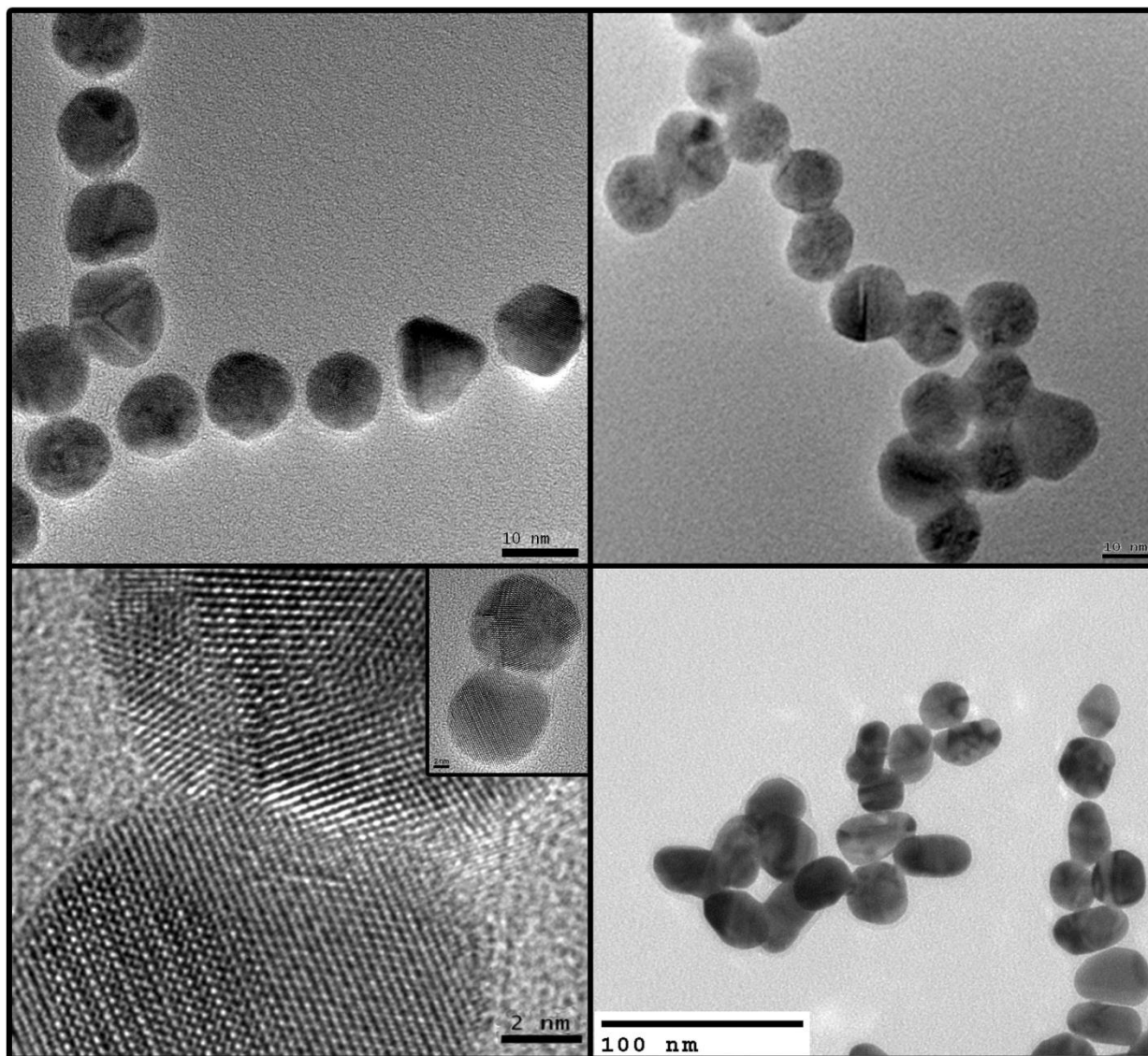


Figure 11. TEM images of A) Au nanospheres B) Au NSDs C) close up of the contacting surfaces of the two spheres that make up the Au NSD, the inset is a zoomed out look at the NP D) TEM of NSDs created with 20 nm citrate Au nanospheres.

To further investigate whether two spheres have physically connected, a high-resolution TEM image was taken focusing on the joint in between the two Au nanospheres. In Figure 11c the crystal structure of Au of each nanosphere can be seen to merge together at the joint, indicating that this is one single fused NP. Additional TEM images of a dimer and trimer are shown in Figure 12a and Figure 12b, respectively. The junctions of the dimer and trimer are similar in that they seem to have different sections of the lattice of each nanosphere “reaching” into the adjacent nanosphere. This is characteristic of surface reconstruction as the lattice does not always uniformly reconstruct.

Figure 13 shows an AFM image of the NSD where we can see the two humps of the NSD and the elongated aspect ratio. Importantly, the sectional analysis shows a NP height of 16.518 nm. The increase in length is likely due to the aggregation that occurs during drying of the sample, similar to Figure 11b.



Figure 12. High Resolution TEM of Au NSD and a possible trimer.

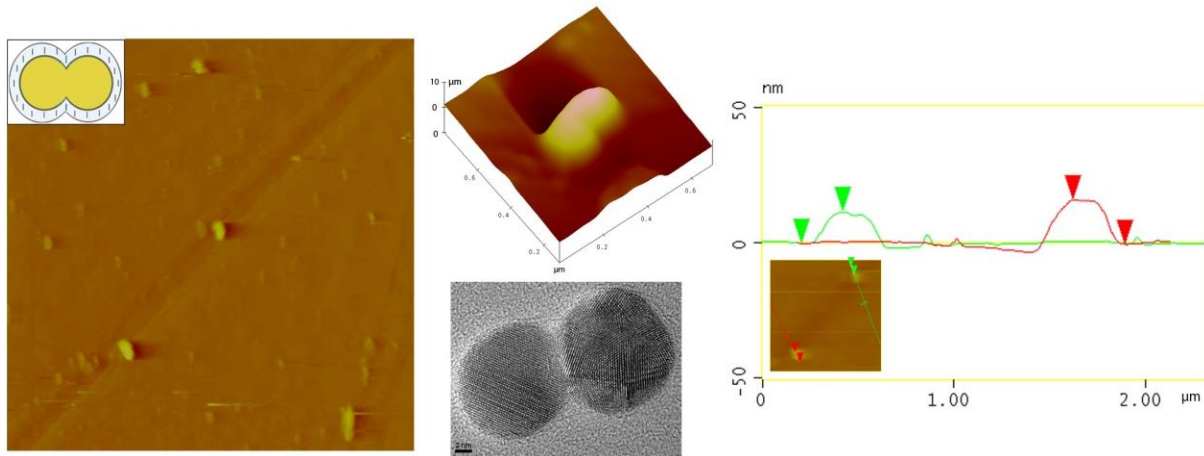


Figure 13. A) Topographic AFM image, B) magnified surface plot from topographic image in Figure 13a C) TEM image of NSD d) AFM sectional analysis result

4.2 Effect of G-Force

In order to investigate the minimum, maximum, and ideal amounts of G-Force to use, the NSD procedure was carried out using 5 cycles and 10 minutes centrifugation times but across different G-Forces. Running at different G-Forces produced absorption curves similar to that seen in Figure 4 except that the relative absorption at 648 nm decreases for G-Forces below 7,500 x g. Figure 14 shows the relative absorption at 648 nm for different G-Forces. As shown, there is no effect when using less than 3,000 x g and no increase in absorbance above 7,500 x g. This was in agreement upon visual inspection as the NSDs under too low of G-Force did not show the same change to blue color as the higher G-Force samples.

Below 3,000 x g, the only contribution to the 648 nm peak seems to be from that of the stock solution which has a slight amount of absorption up to 800 nm. It can be seen from Figure 14 that there is a sharp increase around 3,000 x g which flat-lines around 7,500 x g. This data is also in agreement with a further study at 45,000 x g and 75,000 x g which showed no additional effect on the relative peak height or wavelength with the substantial increase in G-Force shown in Figure 15. It is important to note, however, that the ultra-high G-Force achieved the same absorbance intensity in 2 cycles that normally takes 3 or 4 cycles at 15,000 x g. This goes well with the story of how these NSDs are formed: higher G-Force will bring the Au nanospheres into contact much faster than lower G-Force and perhaps removes the citrate at the junction quicker due to the increased pressure. The results from Figure 14 and Figure 15 lead to the conclusion that after 7,500 x g, the NSDs have reached their maximum yield due to G-Force. Figure 14 also suggests that there may be a minimum requirement of G-Force before the NSD synthesis can even occur.

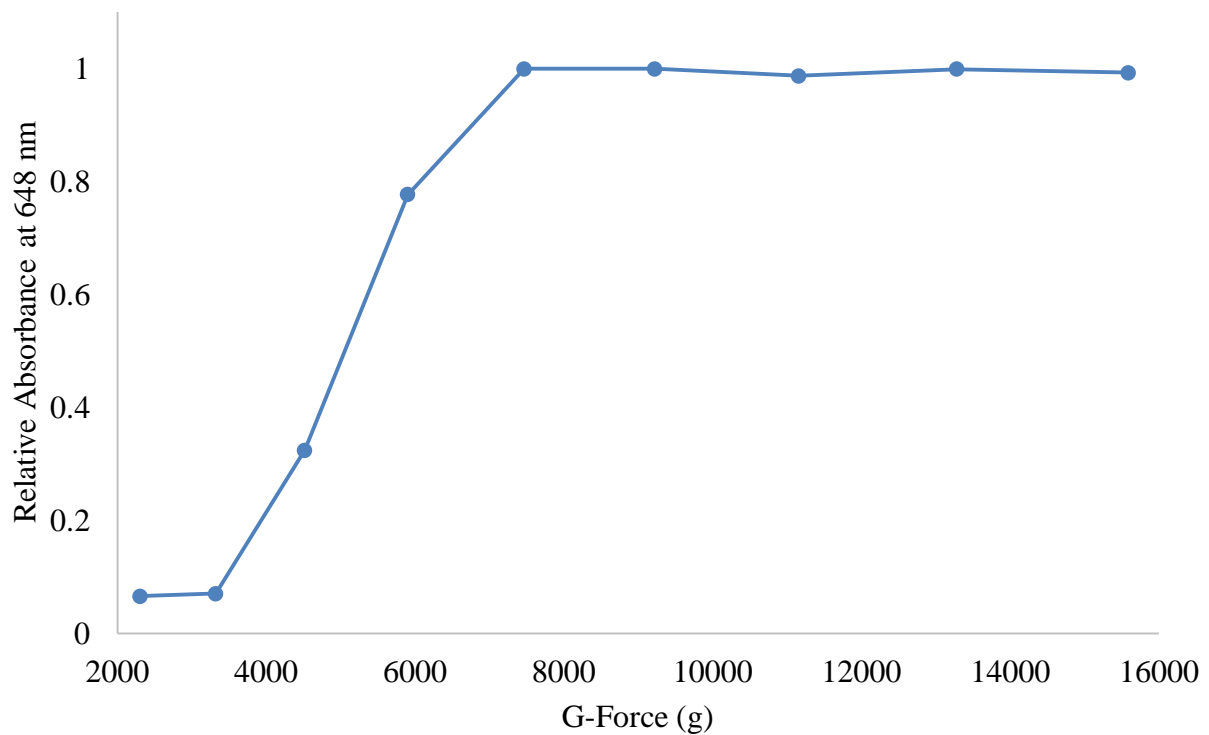


Figure 14. NSD synthesis under varying inertial force. The effect of G-Force on the relative absorbance at 648 nm is shown for NSD samples each synthesized under a different G-Force.

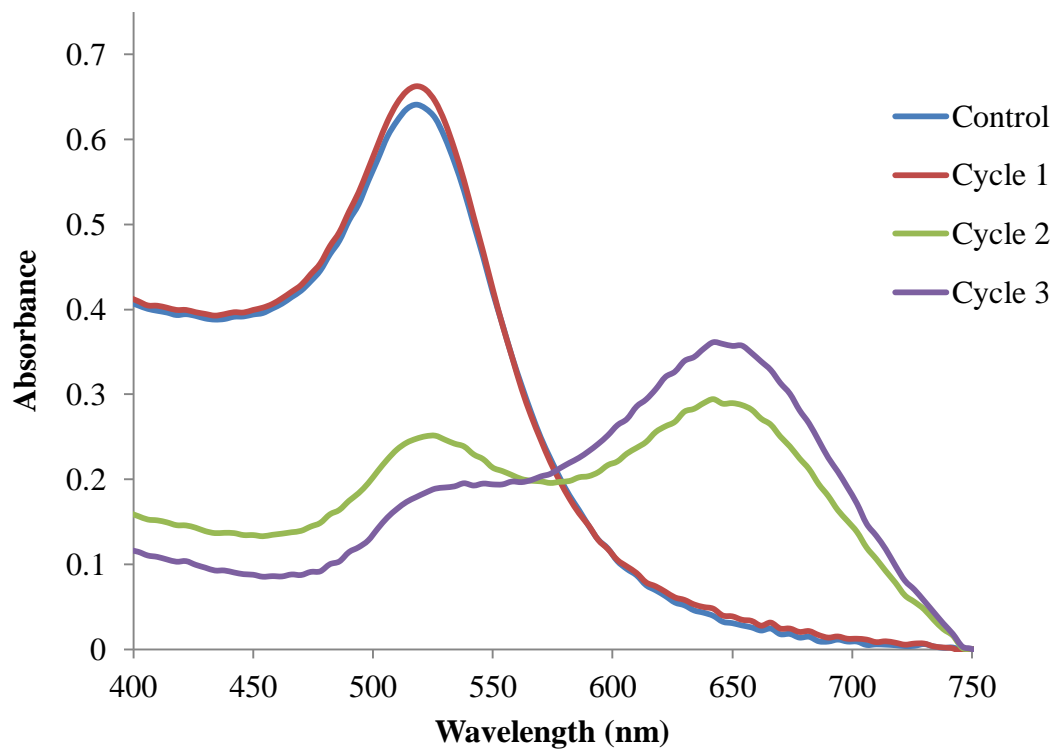


Figure 15. NSDs created using 75,000 x g.

To principally investigate the role of time under a certain G-Force, or cumulative G-Force, the lowest sample from Figure 14, 2,500 x g, was ran again but was put under G-Force for longer, overnight centrifugation times. Figure 16 shows a comparison of two procedures ran at 2,500 x g and 5 cycles: one for 10 minute centrifugation times (red) and one for overnight centrifugations (green). The results show that there was no effect from the 10 minute centrifugations but the overnight centrifugations lead to a moderate increase in the 648 nm peak. This is likely due to sedimentation time which can be roughly calculated using:

$$v = \frac{d^2(p-L) \times g}{18n}$$

where v = sedimentation rate or velocity of the sphere; d = diameter of the sphere; p = particle density; L = medium density; n = viscosity of medium; and g = gravitational force. [109]

Without enough sedimentation time, the particles are not able to physically press together and interact under the G-Force. Cumulative G-Force at 2,500 x g was further investigated by running the NSD procedure through 11 cycles (purple). The purple line in Figure 16 shows that overnight centrifugations lead to a substantial increase in the 648 nm peak and therefore, NSDs were synthesized. Figure 16 shows the importance of centrifugation time and that even under low centrifugation, NSDs can be created. Figure 16 shows that the amount of time spent at a certain G-Force will also play a role in the “quality” of NSDs produced. Possibly, when at low G-force for a long enough time, the Au nanospheres are given ample time to align their crystal structures and fuse together. This is beneficial for practical production as higher G-Force tends to require more specialized and expensive equipment.

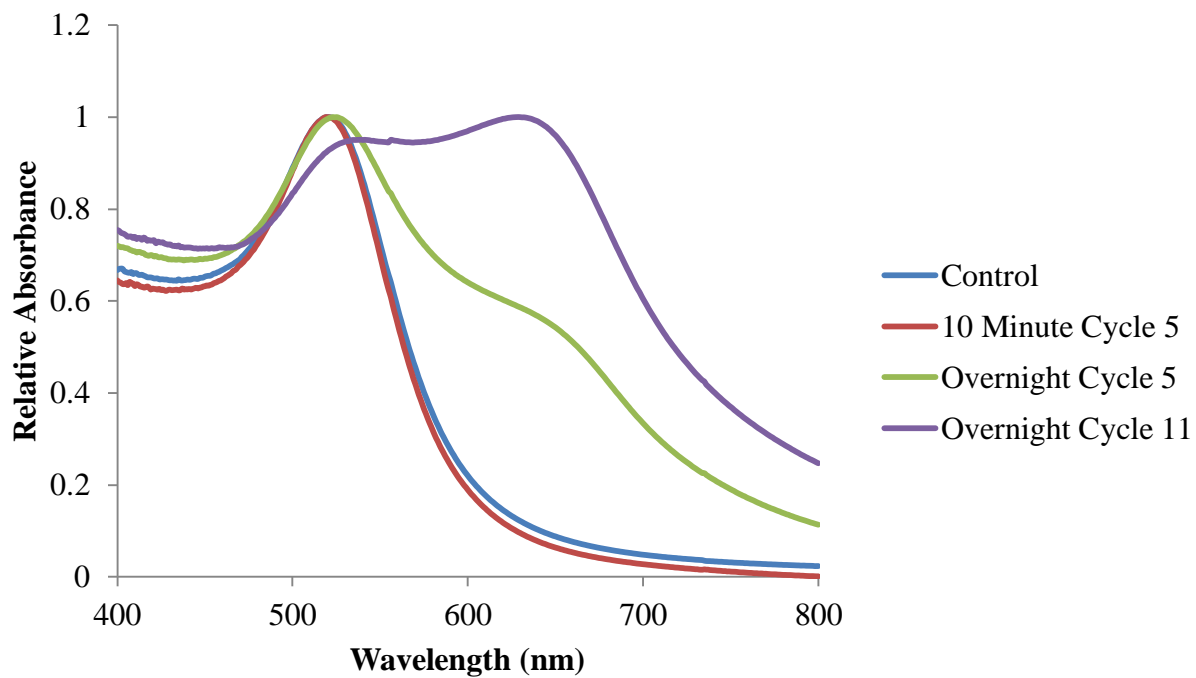


Figure 16. NSDs created using 2,500 x g for overnight centrifugation times.

While searching for the minimum required G-Force to synthesize Au NSDs, the NSD procedure was ran at 1,130 x g for an extended time period of 24 h shown in Figure 17. Running the procedure at 1,130 x g gave a slight broadening of the base of the curve as shown by the orange to purple lines, but only with the additional cycles at the longer time can we finally see a vague bump around the 625 nm range (purple). This bump is likely just an increase in aggregation which may be a formative step for the NSD as similar peaks are seen early cycles of the NSD synthesis procedure. However, after letting the centrifuge run for an additional month, there was a substantial increase in the 580-650 nm range but without any defined peak, indicating that aggregation has occurred rather than NSDs synthesis.

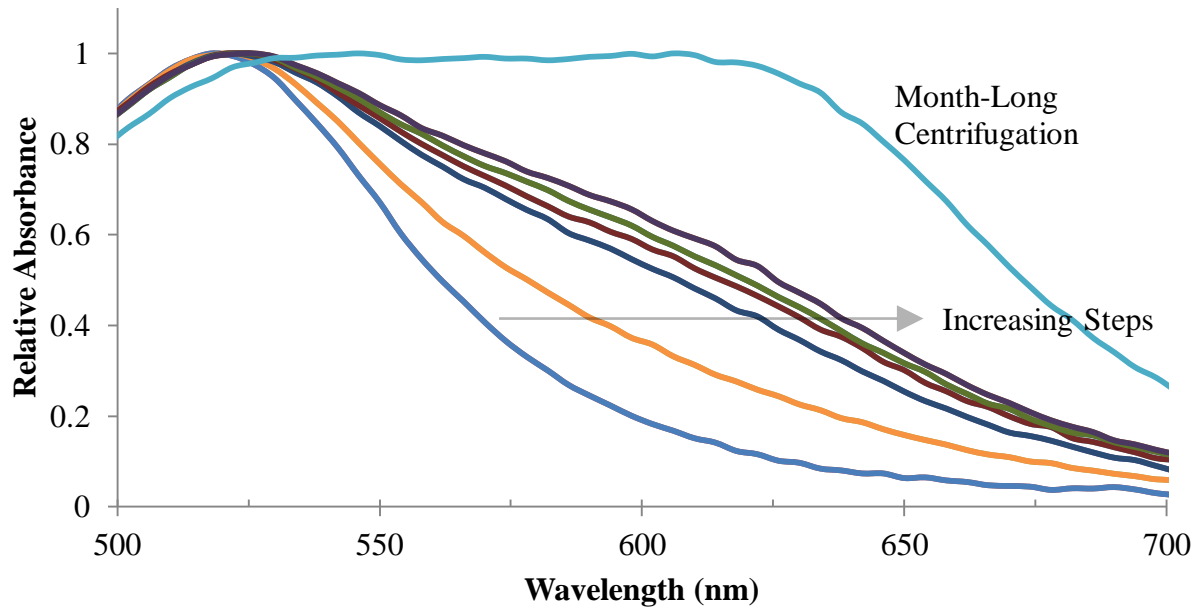


Figure 17. NSD procedure using 1,130 x g and overnight centrifugation times.

4.3 Generalization

Experimental results were compared with theoretical results obtained using the DDA method. The program DDSCAT gave the results shown in Figure 18, which is similar to those obtained by other researchers. [76] The Au nanosphere peaks are both near the 520 nm expected peak and the longitudinal peaks for the NSDs are different by only 6 nm, an error of 0.83%. However, the absorbance intensity differs significantly between experimental and theoretical results. The discrepancies are likely due to the theoretical model being based on perfect spheres, while the actual colloidal samples are only sphere-like. The error may also be due to the number of dipoles chosen, which is limited by available computing power. Higher dipoles will produce more accurate absorbance data. Overall, these results are encouraging and the DDSCAT program may be useful when designing NSDs with different characteristics.

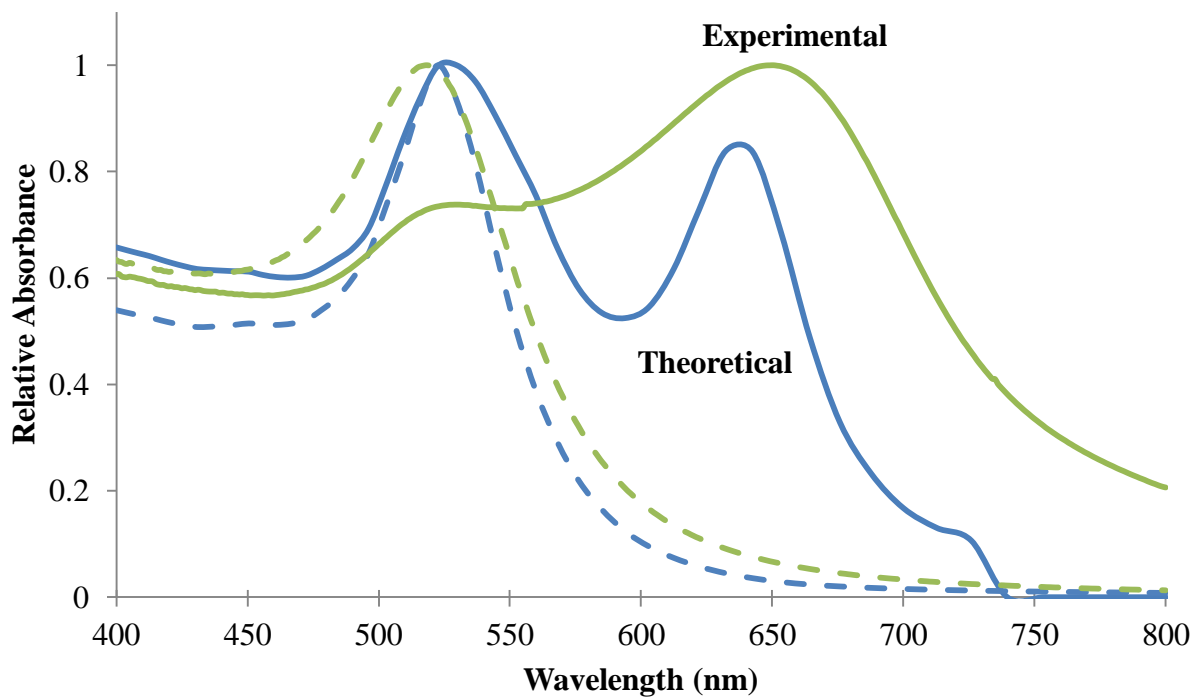


Figure 18. Theoretical Absorbance (blue) compared to experimentally obtained data (green). Dotted lines are spheres, solid lines are dimers.

Figure 19 shows the comparison of the NSD procedure using different size NPs as starting material. The control group on the left shows that the 20 nm Au NPs (orange) have more aggregation than the 14 nm Au NPs (blue). As expected, the mixture of the two control solutions contains an aggregation (red) within the range between the two control solutions. As for the NSD group, all three samples have a SPR peak around 650 nm. This leads us to believe that Au NPs of different sizes can be used to create dimers by following the NSD procedure. More specifically, the pure samples seem to have the same resonance peak while the mixed sample has an even further red-shift. This may be because some of the smaller NPs are bound with the larger, leading to a modified aspect ratio which would result in a red-shift. The mixture of 14 and 20 nm Au NSDs also has a broader peak, suggesting that solution contains NSDs of 14 bound to 14 nm, 14 bound to 20 nm, and 20 bound to 20 nm. Comparing the NSD peaks in orange and red suggest that the increase in aggregation in the mixture is due to both the 20 nm NPs being more aggregated and possibly due to the result of combining multiple sizes. The three NSD samples differ on their 520 nm intensity as a result of unequal separation due to centrifugation because the 20 nm Au NPs are more likely to remain in the solution than the smaller 14 nm NPs which are easily removed. This is validated in Figure 19 by the higher 520 nm peak relative to the 650 nm peak of the pure 20 nm Au NPs (orange) compared to the mixture's 520 nm peak (red).

Figure 11d shows a TEM image of the 20 nm NSDs. Interestingly, there seem to be several cases where the two nanospheres merge completely into each other which may be a result of gold's tendency to reduce curvature. This secondary structure is important because these seem to be more "true" to the GNR morphology suggesting that the NSD procedure may also be creating GNRs without the use of any toxic capping agent. Furthermore, the ability to use

different sizes or mixtures lends itself well to giving the user control and tunability of the NP.

The NSD procedure also worked for larger sizes of Au leading to the conclusion that the size of the NSD is dependent on the size of the starting NPs.

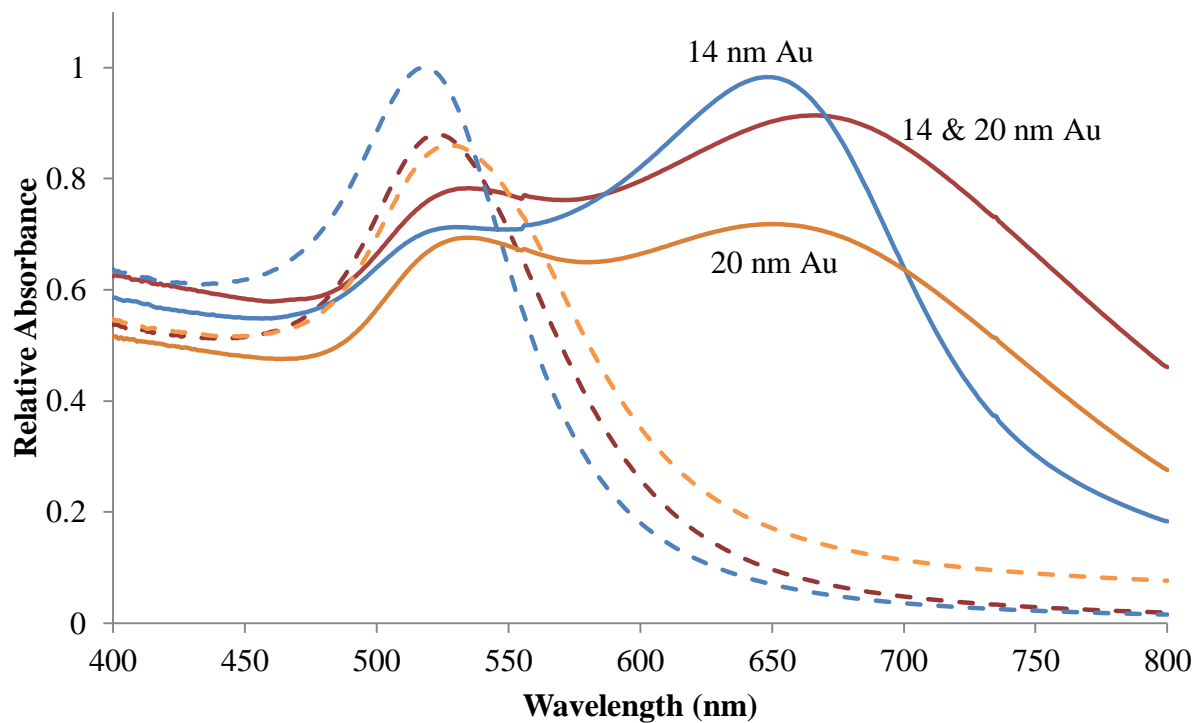


Figure 19. Different sizes of citrate gold used to synthesize NSDs. Starting nanospheres are represented by a dotted line, and their corresponding NSDs are a solid line of the respective color.

Figure 20 shows the comparison of the NSD procedure applied to NPs of different compositions. The dotted line of the colored groups is the wavelength absorption of the starting material while the solid line represents the absorption of the NPs after having gone through the NSD procedure. The magnetic Fe NPs show little effect of NSD procedure though the peak seems to be “cleaner” since the small dual peaks at 230 nm and 246 nm are consolidated at 230 nm. Also, there is a slight broadening of the base of the curve, which may indicate higher aggregation.

The Pt NPs have a clear resonance peak at 230 nm, however, after the NSD procedure there is a broad increase in absorption beyond the 250 nm range which is indicative of aggregation and may contain dimers and trimers. Particularly interesting is the slight peak around 570 nm which indicates that there may be another shape in the NP solution, albeit in low yield. Similarly, Ag NPs showed an increase of intensity at the wavelengths beyond 500 nm; however, there is a more defined curve from 460-660 nm that suggests there may be a significant yield of Ag dimers and trimers. Interestingly, there is actually a slight blue shift of the transverse SPR peak after the NSD procedure. This may be due to the imperfections of the starting solution with the larger, non-spheroid particles aggregating together during centrifugation. Both these findings of the Pt and Ag NSDs are important because they show the potential of the NSD procedure to be a universal mechanism for the simple synthesis of metal NP dimers without the need of any linker.

The last section of Figure 20 compares NSDs synthesized from ATP capped Au NPs and citrate Au NPs. The ATP Au NPs seem to have bound together into dimers as there is a similar SPR red-shift at 626 nm. The difference in the secondary peak as related to that of the citrate Au NPs may be due to the capping agent, difference in size, and difference in starting material preparation. These results look very promising towards a simple, generalized procedure for

fusing two nanospheres together into a single dimer and more importantly, it shows that by changing the capping agent or composition allow for the tuning of nanostructures synthesized according to the NSD procedure.

The results from a preliminary study into the fusion of NPs of two different compositions is shown in Figure 21. The mixture of Ag NPs and citrate Au NPs is shown in blue and both the 420 nm and 520 nm peaks from the Ag and Au, respectively, are present. However, after 6 cycles (orange) of the NSD procedure, there seems to be a broad peak around the 920 nm range. The lighter weight of Ag NPs may be playing a role in sedimentation time and hence, further cycles were necessary. While this data is inconclusive, this is evidence that it may be possible to create hybrid nanostructures with interesting optical properties using this simple synthesis approach.

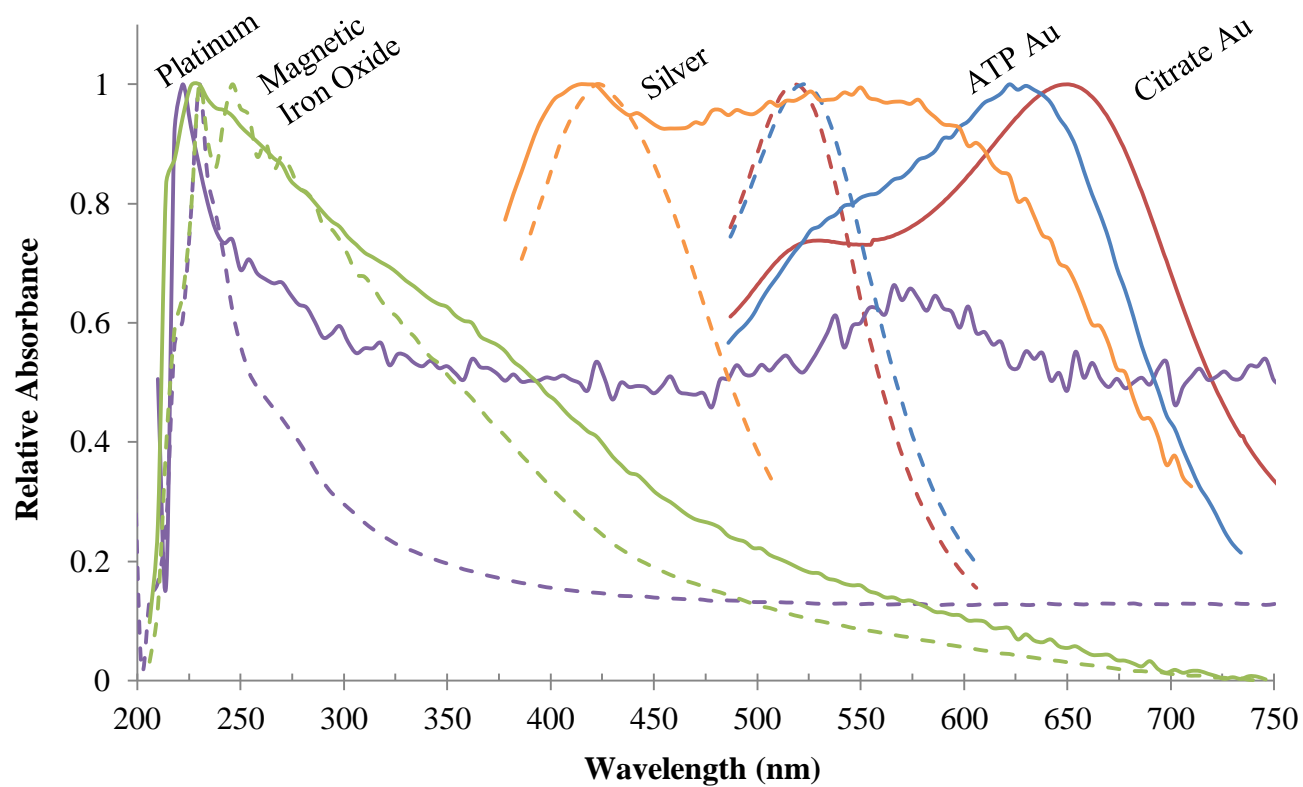


Figure 20. Comparison of the NSD procedure using different metal compositions. The dotted lines show the starting NP absorbance and the solid line of the respective color shows the corresponding shift after the NSD procedure.

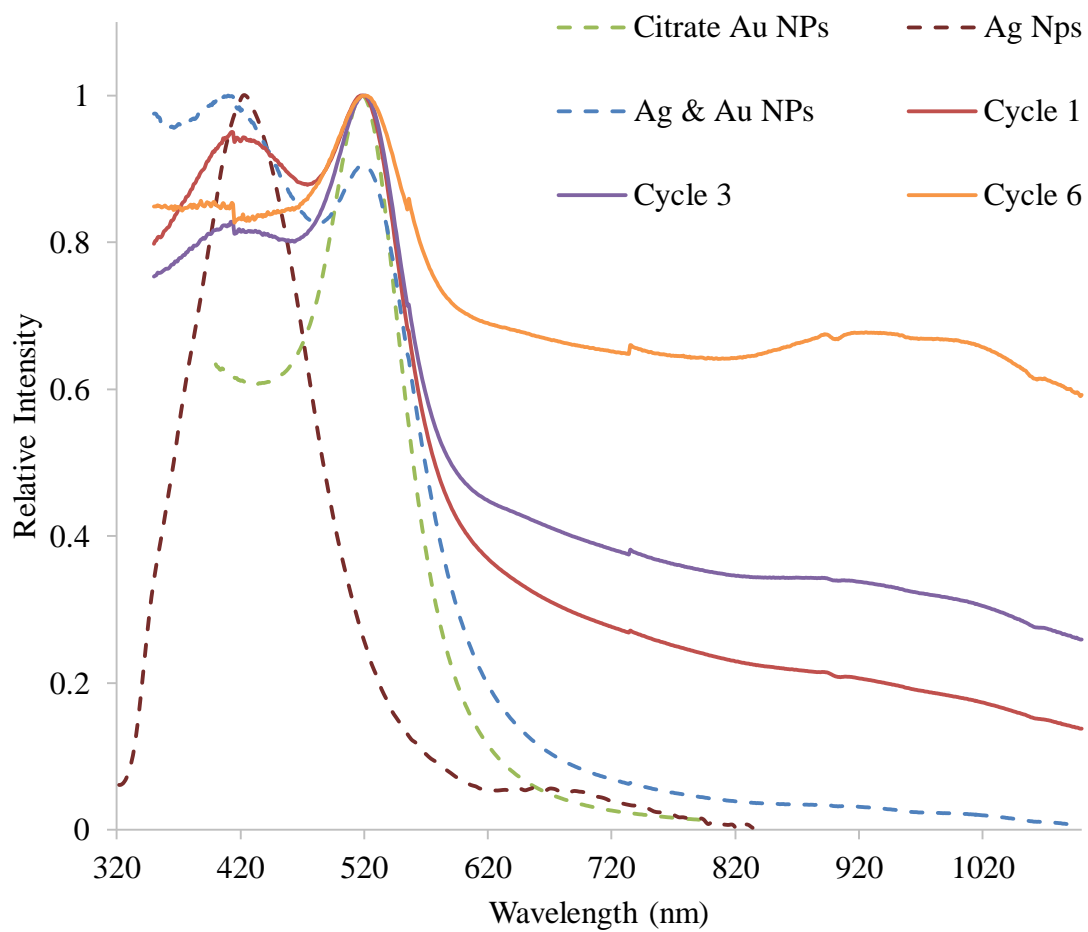


Figure 21. Mixture of Ag and Au NPs to create hybrid nanostructures.

4.4 Mechanism

Figure 22a shows the alignment phase of the NSD procedure: Au nanospheres freely rotate to lowest energy and line up before undergoing surface reconstruction. It is important to note that Au NPs are not perfect spheres and will experience a ‘physical polarization’ and will line up with directionality under immense G-Force. This polarization will actually compress the electrical double-layer of the NPs, and as seen in other research, the electrical layer overlap can cause clusters due to the weakened repulsion and dominance of van der Waals forces. [26]

Figure 22b shows the citrate coating of two Au NPs merging under high centrifugation and low surrounding solution concentration of citrate. When the concentration of citrate in solution is lowered, the charge of the solution changes and allows the nanospheres to combine without the excess citrate “slipping in” between them. There may be less steric hinderence surrounding the individual nanospheres and hence the repulsion of the citrate of two different spheres is not strong enough to keep the Au cores from touching. With less hinderence and shorter interparticle distance, the Casimir effect may also come into play, instantaneously bringing the NPs together.

Once the polarized ends fix their position, surface reconstruction may take place at the junction between the two spheres to achieve chemical and electrical stability as described by Figure 22c. This creates a physical/chemical bond between the two nanosphere cores. A portion of the negatively charged citrate coating, that previously existed between the two cores, shifts to surround the newly fused, positively charged dimer core which may contribute to a larger layer of citrate surrounding the NSD than the starting nanosphere.

This may contribute to the explanation of why further aggregation does not occur: the steric hindrance of the large citrate layers around the NSD and the increased electrostatic repulsion are too strong. During the first cycles of high centrifugation, the bulk of citrate is removed during the capping agent replacement step. With lower citrate concentration and continued G-force, citrate is squeezed out of the intersection of the two nanospheres and surrounds the NP along with the rest of the citrate remaining in solution. As the citrate is attracted to Au surface, it creates additional electrostatic repulsion and steric hindrance for the individual NSDs. Furthermore, NSDs may not easily bind to other NSDs because of physical hindrance during the alignment phase. The end result is a physically, chemically, and electrically stable NP.

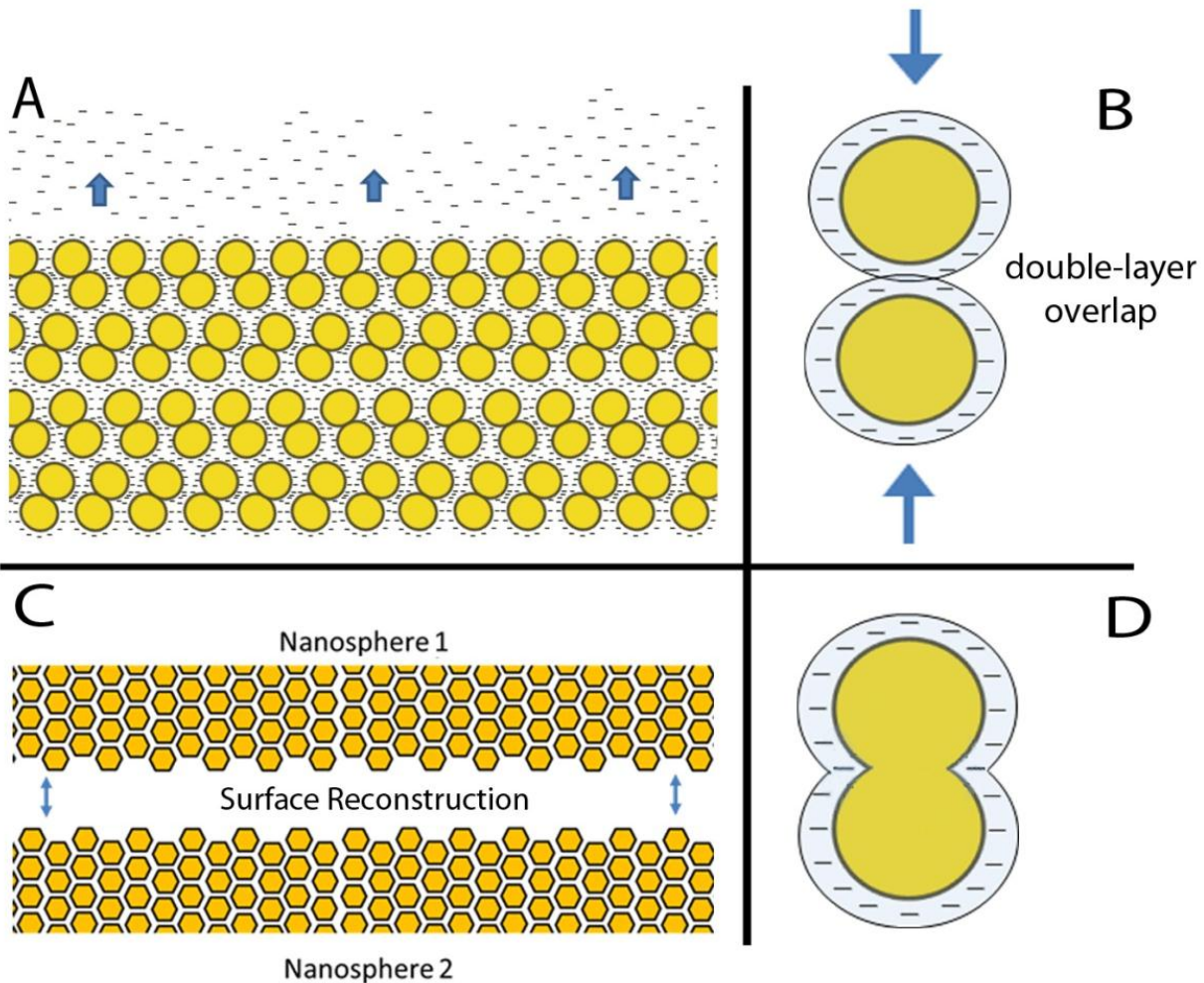


Figure 22. Proposed NSD mechanism. a) Alignment phase: Au nanospheres freely rotate to their lowest energy and line up before undergoing surface reconstruction b) Citrate coating of two Au NPs merges under high centrifugation and low surrounding solution concentration of citrate. Under the right conditions, the repulsion of the citrate of two different spheres is not strong enough to keep the Au cores from touching, c) Surface reconstruction begins at the junction between the two spheres d) The result is a physically, chemically, and electrically stable NP. The crystal alignment can be seen from the TEM result in Figure 11c.

Chapter 5: Conclusions

A method for controllable and tunable nanostructures as well as the synthesis of Au NSDs in high yield has been described. NSDs have potential application in electronics, sensing, and biological applications due their simple surfaces, flexibility of size, and absorbance at the NIR range. The procedure is cost-effective and relatively simple, meaning less can go wrong particularly during functionalization steps or *in vivo* applications. These advantages make NSDs an attractive alternative to GNRs. Furthermore, it is possible to create NSDs of different sizes and compositions.

Popular NPs with different plasmonic responses were also investigated and showed a significant change in absorbance, indicating that this method can be generalized across NPs of different compositions. This alone is worth further investigation as it allows researchers access to a new variety of morphologies with tuned plasmonic responses. Modeling with computational methods may aid in the “tuning” of the precise dimer shape in order to achieve an SPR at a particular frequency.

This is the first known case to the author of two Au nanospheres combining at their crystal lattice surfaces into a dimer without the use of a chemical linker NP. It is hypothesized that attractive van der Waals and repulsive electrical double layer forces exchange dominance to allow the stability and formation of Au NSDs. An applied G-Force polarizes the NPs which reduces the electrical double layer, allowing van der Waal’s forces to prevail and bring the surfaces in contact and causes the NPs to undergo surface reconstruction at the junction. The presence of the capping ligand may play a key role in the electrostatic forces that bind the two spheres into a

single, stabilized dimer. Further investigation into the role of quantum phenomena and entropy may reveal the importance of other binding forces such as the Casimir effect.

TEM and AFM images confirmed the creation of the NSD shape and suggest that there is physical attachment at the junction between the two nanospheres. This junction should be studied in more detail with techniques such as X-ray diffraction. Optical spectra analysis showed a transverse axis wavelength band at about 520 nm and a longer wavelength in the NIR region with a peak at about 650 nm which is attributed to the longitudinal SPR. A statistical analysis of the distribution of NSDs is needed as well as a study into what percent of trimers, if any, exist in the solution,

The SPR achieved should allow NSDs to be irradiated by a NIR laser for use in photoacoustic/photothermal theranostics *in vivo*. The simplicity of the NSDs make them ideal for functionalization strategies for cell targeting and drug delivery. Further study into their optical properties as a function of their aspect ratio and size may show the advantage of increased surface area. This would allow easier detection of CTCs as a stronger photoacoustic signal would be produced.

NSDs may have even better function as isotropic contrast agents and may provide enhancements in electron microscopy, electronics, phototherapy, and materials science. Their controllability and tunability make this procedure attractive to many fields as NPs can be fabricated with custom properties in mind. The exact mechanism by which these particles are made is still under investigation but a possible mechanism has been suggested. There is also interest in determining additional properties that may be unique to these particles as well as the result of combining other nano-morphologies and compositions together in similar procedures. This research

reiterates the strange phenomena at the nanoscale and as our understanding continues, mankind will be able to create a myriad of materials with potentially infinite applications.

5.1 Future Recommendations

There are many different aspects of this research that can be further investigated, some are large projects in their own right. Different capping agents, NP shapes, compositions, and mixtures should be explored for their role in tuning. Removal of the capping agent, changes in pH and temperature should be tested as they could elucidate the mechanism and provide a means for additional assembly or structure formation such as trimers, tetramers, or entirely different shapes.

Further study into the relationship between time, G-Force, repetitions, and concentration could eventually be used to create a model to predict the necessary requirements to make NSDs given a certain constraint. Additional imaging and statistical analysis of NSDs and NP solutions could also help in quantifying the outcomes of the particular procedure. Particularly, the crystal structure at the junction of the NSD should be deeply studied through further high-resolution TEM and X-ray diffraction. Finally, calculation of electrostatic, van der Waals, entropic, and possible Casimir forces could give a precise understanding of the energy involved in the NSD mechanism.

Works Cited

- [1] L. Vigderman, P. B. Khanal and R. E. Zubarev, "Functional Gold Nanorods: Synthesis, Self-Assembly, and Sensing Applications," *Advanced Materials*, no. 24, pp. 4811-4841, 2012.
- [2] J.-W. Kim and R. Deaton, "Molecular self-Assembly of multifunctional nanoparticle composites with arbitrary shapes and functions: challenges and strategies," *Particle & Particle Systems Characterization*, vol. 30, pp. 117-132, 2013.
- [3] J. Shao, R. J. Griffin, E. I. Galanzha, J.-W. Kim, N. Koonce, J. Webber, T. Mustafa, A. S. Biris, D. A. Nedosekin and V. P. Zharov, "Photothermal nanodrugs: potential of TNF-gold nanospheres for cancer theranostics," *Scientific Reports*, vol. 3, pp. 1-9, 2013.
- [4] N. Kotagiri and J. Kim, "Stealth theranostic agents: strategies of shielding carbon nanotubes and their hybrids to evade opsonization and improve biodistribution," *International Journal of Nanomedicine*, vol. 9, no. S1, pp. 58-105, 2014.
- [5] J.-W. Kim, E. I. Galanzha, D. Zaharoff, R. J. Griffin and V. P. Zharov, "Nanotheranostics of circulating tumor cells, infection and other pathological features in vivo," *Molecular Pharmaceuticals*, vol. 10, pp. 813-830, 2013.
- [6] A. de la Zerda, J.-W. Kim, E. I. Galanzha, S. S. Gambhir and V. P. Zharov, "Advanced contrast nanoagents for photoacoustic molecular imaging, cytometry, blood test, and photothermal theranostics," *Contrast Media & Molecular Imaging*, vol. 6, pp. 346-369, 2011.
- [7] S. D. Brown, P. Nativo, J.-A. Smith, D. Stirling, P. R. Edwards, B. Venugopal, D. J. Flint, J. A. Plumb, G. Duncan and N. J. Wheate, "Gold Nanoparticles for the Improved Anticancer Drug Delivery of the Active Component of Oxaliplatin," *Journal of the American Chemical Society*, vol. 132, pp. 4678-4684, 2010.
- [8] E. Galanzha, J. Kim and V. Zharov, "Nanotechnology-based molecular photoacoustic and photothermal flow cytometry platform for in-vivo detection and killing of circulating cancer stem cells," *Journal of Biophotonics*, vol. 2, no. 12, pp. 725-735, 2009.
- [9] E. Galanzha, M. Kokoska, E. Shashkov, J. Kim, V. Tuchin and V. Zharov, "In vivo fiber-based multicolor photoacoustic detection and photothermal purging of metastasis in sentinel lymph nodes targeted by nanoparticles," *Journal Of Biophotonics*, no. 9, pp. 528-539, 2009.

- [10] J.-W. Kim, J.-H. Kim and R. Deaton, "DNA-Linked Nanoparticle Building Blocks for Programmable Matter," *Angewandte Chemie*, vol. 50, pp. 9185-9190, 2011.
- [11] L. C. Brousseau III, J. P. Novak, S. M. Marinakos and D. L. Feldheim, "Assembly of Phenylacetylene-Bridged Gold Nanocluster Dimers and Trimers," *Advanced Materials*, vol. 11, no. 6, pp. 447-449, 1999.
- [12] Y. Jung, H. Chen, L. Tong and J.-X. Cheng, "Imaging Gold Nanorods by Plasmon-Resonance-Enhanced Four Wave Mixing," *Journal of Physical Chemistry*, vol. 113, pp. 2657-2663, 2009.
- [13] American Cancer Society, "Cancer Facts & Figures 2014," American Cancer Society, Atlanta, GA, 2014.
- [14] J.-W. Kim, E. I. Galanzha, E. V. Shashkov, H.-M. Moon and V. P. Zharov, "Golden carbon nanotubes as multimodal photoacoustic and photothermal high-contrast molecular agents," *Nature Nanotechnology*, vol. 4, no. 10, pp. 688-694, 2009.
- [15] C. Song, Z. Wang, R. Zhang, J. Yang, X. Tan and Y. Cui, "Highly sensitive immunoassay based on Raman reporter-labeled immuno-Au aggregates and SERS-active immune substrate," *Biosensors and Bioelectronics*, vol. 25, pp. 826-831, 2009.
- [16] E. I. Galanzha, E. Shashkov, M. Sarimollaoglu, K. E. Beenken, A. G. Basnakian, M. E. Shirtliff, J.-W. Kim, M. S. Smeltzer and V. P. Zharov, "In Vivo Magnetic Enrichment, Photoacoustic Diagnosis, and Photothermal Purging of Infected Blood Using Multifunctional Gold and Magnetic Nanoparticles," *PLOS One*, vol. 7, no. 9, pp. 1-14, 2012.
- [17] E. Galanzha, E. Shashkov, T. Kelly, J.-W. Kim, L. Yang and V. P. Zharov, "Integrated nanotechnology-based photoacoustic and photothermal flow cytometry platform for in vivo detection and killing of circulating cancer stem cells," *Nature Nanotechnology*, vol. 4, pp. 855-860, 2009.
- [18] J.-W. Kim, E. V. Shashkov, E. I. Galanzha, N. Kotagiri and V. P. Zharov, "Photothermal Antimicrobial Nanotherapy and Nanodiagnostics With Self-Assembling Carbon Nanotube Clusters," *Lasers in Surgery and Medicine*, vol. 39, pp. 622-634, 2007.
- [19] E. Fourkal, I. Velchev, A. Taffo, C. Ma, V. Khazak and N. Skobeleva, "Photo-Thermal Cancer Therapy Using Gold Nanorods," *World Congress on Medical Physics and Biomedical Engineering*, vol. 25, pp. 761-763, 2009.

- [20] G. von Maltzahn, A. Centrone, J.-H. Park, R. Ramanathan, M. J. Sailor, T. A. Hatton and S. N. Bhatia, "SERS-Coded Gold Nanorods as a Multifunctional Platform for Densely Multiplexed Near-Infrared Imaging and Photothermal Heating," *Advanced Materials*, vol. 21, pp. 3175-3180, 2009.
- [21] V. P. Zharov, J.-W. Kim, D. T. Curiel and M. Everts, "Self-assembling nanoclusters in living systems: application for integrated photothermal nanodiagnostics and nanotherapy," *Nanomedicine*, vol. 1, pp. 326-345, 2005.
- [22] V. P. Zharov, E. I. Galanzha, E. V. Shashkov, J.-W. Kim, N. G. Khlebtsov and V. V. Tuchin, "Photoacoustic flow cytometry: principle and application for real-time detection of circulating single nanoparticles, pathogens, and contrast dyes in vivo," *Journal of Biomedical Optics*, vol. 12, no. 5, pp. 1-13, 2007.
- [23] G. Mie, "Contributions to the optics of turbid media, particularly colloidal metal suspensions," *Annalen der Physik*, vol. 25, no. 3, pp. 377-445, 1908.
- [24] R. Gans, "The form of ultramicroscopic gold particles," *Annalen der Physik*, vol. 342, no. 5, pp. 881-900, 1912.
- [25] S. Link and M. A. El-Sayed, "Size and Temperature Dependence of the Plasmon Absorption of Colloidal Gold Nanoparticles," *J Phys Chem*, vol. B, no. 103, pp. 4212-4217, 1999.
- [26] M. Roca, N. H. Pandya, S. Nath and A. J. Haes, "Linear Assembly of Gold Nanoparticle Clusters via Centrifugation," *Langmuir*, vol. 26, no. 3, pp. 2035-2041, 2009.
- [27] K. M. Mayer, F. Hao, S. Lee, P. Nordlander and J. Hafner, "A single molecule immunoassay by localized surface plasmon resonance," *Nanotechnology*, vol. 21, pp. 1-8, 2010.
- [28] A. J. Haes and R. P. Van Duyne, "A Nanoscale Optical Biosensor: Sensitivity and Selectivity of an Approach Based on the Localized Surface Plasmon Resonance Spectroscopy of Triangular Silver Nanoparticles," *Journal of the American Chemical Society*, vol. 124, pp. 10596-10604, 2002.
- [29] W. Cai, T. Gao, H. Hong and J. Sun, "Applications of gold nanoparticles in cancer nanotechnology," *Nanotechnology, Science and Applications*, vol. 1, pp. 17-32, 2008.
- [30] A. M. Alkilany, S. E. Lohse and C. J. Murphy, "The Gold Standard: Gold Nanoparticle Libraries To Understand the Nano-Bio Interface," 2012.

- [31] J.-H. Kim and J.-W. Kim, "Sequential Solid-Phase Fabrication of Bifunctional Anchors on Gold Nanoparticles for Controlable and Scalable Nanoscale Structure Assembly," *Langmuir*, vol. 24, pp. 5667-5671, 2008.
- [32] J.-H. Kim and J.-W. Kim, "Simultaneously controlled directionality and valency on a water-soluble gold nanoparticle precursor for aqueous-phase anisotropic self-assembly," *Langmuir*, vol. 26, pp. 18634-18638, 2010.
- [33] J.-W. Kim, J.-H. Kim and R. Deaton, "Programmable construction of nanostructures: assembly of nanostructures with various nanocomponents," *IEEE Nanotechnology*, vol. 6, no. 1, pp. 19-23, 2012.
- [34] A. Murray and W. L. Barnes, "Plasmonic Materials," *Advanced Materials*, no. 12, pp. 3771 - 3782, 2007.
- [35] S. M. Marinakos, S. Chen and A. Chilkoti, "Plasmonic Detection of a Model Analyte in Serum by a Gold Nanorod Sensor," *Analytical Chemistry*, vol. 79, no. 14, pp. 5278-5283, 2007.
- [36] R. F. Knarr, R. A. Quon and T. K. Vanderlick, "Direct Force Measurements at the Smooth Gold/Mica Interface," *Langmuir*, vol. 14, pp. 6414-6418, 1998.
- [37] L. Chen, J. M. Mccrate, J. C.-M. Lee and H. Li, "The role of surface charge on the uptake and biocompatibility of hydroxyapatite nanoparticles with osteoblast cells," *Nanotechnology*, vol. 22, pp. 1-10, 2011.
- [38] G. Schatz, M. A. Young and R. P. Van Duyne, "Electromagnetic Mechanism of SERS," *Topics Appl Phys.*, no. 103, pp. 19-46, 2006.
- [39] R. A. Alvarez-Puebla, E. R. Zubarev, N. A. Kotov and L. M. Liz-Marzan, "Self-assembled nanorod supercrystals for ultrasensitive SERS diagnostics," *Nano Today*, vol. 7, pp. 6-9, 2012.
- [40] J. Hu, L. Lu, W. He, J. Pan, W. Wang and J. Xiang, "Ligand exchange based water-soluble, surface-enhanced Raman scattering-tagged gold nanorod probes with improved stability," *Chemical Physics Letters*, vol. 513, pp. 241-245, 2011.
- [41] R. A. Alvarez-Puebla, A. Agarwal, P. Manna, B. P. Khanal, P. Aldeanueva-Potel, E. Carbo-Argibay, N. Pazos-Perez, L. Vigderman, E. R. Zubarev, N. A. Kotov and L. M. Liz-Marzan, "Gold nanorods 3D-supercrystals as surface enhanced Raman scattering spectroscopy substrates for the rapid detection of scrambled prions," *PNAS*, vol. 108, no.

- 20, pp. 8157-8161, 2011.
- [42] J. A. Dougan and K. Faulds, "Surface enhanced Raman scattering for multiplexed detection," *Analyst*, vol. 137, no. 3, pp. 545-554, 2012.
- [43] R. Weissleder, "A clearer vision for in vivo imaging," *Nature Biotechnology*, vol. 19, pp. 316-317, 2001.
- [44] C. E. Rayford II, G. Schatz and K. Shuford, "Optical Properties of Gold Nanospheres," *Nanoscape*, vol. 2, no. 1, pp. 27-33, 2005.
- [45] E. I. Galanzha, E. V. Shashkov, T. Kelly, J.-W. Kim, L. Yang and V. P. Zharov, "In vivo magnetic enrichment and multiplex photoacoustic detection of circulating tumour cells," *Nature Nanotechnology*, vol. 4, pp. 855-860, 2009.
- [46] G. Gupta and J. Massague, "Cancer metastasis: building a framework," *Cell*, vol. 127, pp. 679-695, 2006.
- [47] I. Fidler, "Metastasis: Quantitative Analysis of Distribution and Fate of Tumor Emboli Labeled with ¹²⁴I-5-iodo-2'-deoxyuridine," *J Natle Cancer Inst*, vol. 45, pp. 773-782, 19701.
- [48] R. R. Langley and I. J. Fidler, "The seed and soil hypothesis revisited - the role of tumor-stroma interactions in metastasis to different organs," *Int J Cancer*, vol. 128, no. 11, pp. 2527-2535, 2011.
- [49] H. M. Shapiro, *Practical Flow Cytometry*, New Jersey: John Wiley & Sons, Inc., 2003.
- [50] J. P. Pawley, *Handbook of Biological and Confocal Microscopy*, 2nd edn, New York: Plenum, 1995.
- [51] J. Turkevich, P. C. Stevenson and J. Hillier, "A Study of the Nucleation and Growth Processes in the Synthesis of Colloidal Gold," *Duscussions of the Faraday Society*, vol. 11, pp. 55-75, 1951.
- [52] J. Polte, T. T. Ahner, F. Delissen, S. Sokolov, F. Emmerling, A. F. Thunemann and R. Kraehnert, "Mechanism of Gold Nanoparticle Formation in the Classical Citrate Synthesis Method Derived from Coupled In Situ XANES and SAXS Evaluation," *Journal of the American Chemical Society*, vol. 132, pp. 1296-1301, 2010.
- [53] D. Huang, F. Liao, S. Molesa, D. Redinger and V. Subramanian, "Plastic-Compatible Low Resistance Printable Gold Nanoparticle Conductors for Flexible Electronics," *Journal of*

- the Electrochemical Society*, vol. 150, no. 7, pp. 412-417, 2003.
- [54] R. K. Visaria, R. J. Griffin and B. W. Williams, "Enhancement of tumor thermal therapy using gold nanoparticle-assisted tumor necrosis factor α delivery," *Molecular Cancer Therapeutics*, vol. 5, pp. 1014-1020, 2006.
- [55] P. L. Truong, C. Cao, S. Park, M. Kim and S. J. Sim, "A new method for non-labeling attomolar detection of diseases based on an individual gold nanorod immunosensor," *Lab on a Chip*, vol. 11, no. 15, pp. 2591-2597, 2011.
- [56] P. L. Truong, B. W. Kim and S. J. Sim, "Rational aspect ratio and suitable antibody coverage of gold nanorod for ultra-sensitive detection of a cancer biomarker," *Lab on a Chip*, vol. 12, no. 6, pp. 1102-1109, 2012.
- [57] N. R. Jana, L. Gearheart and C. J. Murphy, "Seed-Mediated Growth Approach for Shape Controlled Synthesis of Spheroidal and Rod-like Gold Nanoparticles Using a Surfactant Template," *Advanced Materials*, vol. 13, no. 18, pp. 1389-1393, 2001.
- [58] X. Huang, I. H. El-Sayed, W. Qian and M. El-Sayed, "Cancer Cells Assemble and Align Gold Nanorods Conjugated to Antibodies to Produce Highly Enhanced, Sharp, and Polarized Surface Raman Spectra: A Potential Cancer Diagnostic Marker," *Nano Letters*, vol. 7, no. 6, pp. 1591-1597, 2007.
- [59] E. Hao and G. C. Schatz, "Electromagnetic fields around silver nanoparticles and dimers," *The Journal of Chemical Physics*, vol. 120, no. 1, pp. 357-366, 2004.
- [60] B. Li and C. Y. Li, "Immobilizing Au Nanoparticles with Polymer Single Crystals, Patterning and Asymmetric Functionalization," *Journal of American Chemical Society*, vol. 129, pp. 12-13, 2007.
- [61] Y. Liu and V. Ozolins, "Self-Assembled Monolayers on Au(111): Structure, Energetics, and Mechanism of Reconstruction Lifting," *The Journal of Physical Chemistry*, vol. 116, pp. 4738-4747, 2012.
- [62] R. Sardar, T. B. Heap and J. S. Shumaker-Parry, "Versatile Solid Phase Synthesis of Gold Nanoparticle Dimers Using an Asymmetric Functionalization Approach," *JACS Communications*, no. 129, pp. 5356-5357, 2007.
- [63] C. J. Loweth, W. B. Caldwell, X. Peng, A. P. Alivisatos and P. G. Schultz, "DNA-Based Assembly of Gold Nanocrystals," *Angewandte Chemie International Edition*, vol. 38, no. 12, pp. 1808-1812, 1999.

- [64] J. G. Worden, A. W. Shaffer and Q. Huo, "Controlled functionalization of gold nanoparticles through a solid phase synthesis approach," *Chemical Communications*, pp. 518-519, 2004.
- [65] A. L. Tchebotareva, P. V. Ruijgrok, P. Zijlstra and M. Orrit, "Probing the acoustic vibrations of single metal nanoparticles by ultrashort laser pulses," *Laser & Photonics Review*, vol. 4, no. 5, pp. 581-597, 2009.
- [66] E. C. Le Ru and P. G. Etchegoin, *Principles of Surface-Enhanced Raman Spectroscopy*, Amsterdam: Elsevier B.V., 2009.
- [67] G. A. C. Sakhel, "The Role of Surface Plasmons in Nanoscience," 2012.
- [68] R. B. M. & Schasfoort and A. J. Tudos, *Handbook of surface plasmon resonance*, Cambridge, UK: RSC Pub, 2008.
- [69] M. R. Jones, K. D. Osberg, R. J. Macfarlane, M. R. Langille and C. A. Mirkin, "Templated Techniques for the Synthesis and Assembly of Plasmonic Nanostructures," *Chemical Reviews*, no. 111, pp. 3736-3827, 2011.
- [70] J. Hart and A. Schmidt, "Surface Plasmon Resonance and Energy Transfer," University of Michigan, Michigan, 2010.
- [71] G. A. C. Sakhel, "The Role of Surface Plasmons in Nanoscience," Unpublished Manuscript, University of Arkansas, Fayetteville, 2012.
- [72] K. L. Kelly, E. Coronado, L. L. Zhao and S. C. George, "The Optical Properties of Metal Nanoparticles: The Influence of Size, Shape, and Dielectric Environment," *J Phys Chem B*, vol. 107, no. 3, pp. 668-667, 2003.
- [73] V. K. Komarala, W.-H. Guo and M. Xiao, "Surface plasmon density of states at the metal-dielectric interface: Dependence of metal layer thickness and dielectric material," *Journal of Applied Physics*, no. 107, pp. 014309-1 - 014309-5, 2010.
- [74] C. E. Talley, J. B. Jackson, C. Oubre, N. K. Grady, C. W. Hollars, S. M. Lane, T. R. Huser, P. Nordlander and N. J. Halas, "Surface-Enhanced Raman Scattering from Individual Au Nanoparticles and Nanoparticle Dimer Substrates," *Nano Letters*, vol. 5, no. 8, pp. 1569-1574, 2005.
- [75] E. M. Purcell and C. R. Pennypacker, "Scattering and absorption of light by nonspherical dielectric grains," *The Astrophysical Journal*, vol. 186, pp. 705-714, 1973.

- [76] M. J. Crow, *Molecular imaging and sensing using plasmonic nanoparticles*, Ann Arbor, MI: ProQuest, UMI Dissertations Publishings, 2010.
- [77] C. Ungureanu, R. G. Rayavarapu, S. Manohar and T. G. Leeuwen, "Discrete Dipole Approximation simulations of gold nanorod optical properties: choice of input parameters and comparison with experiment," *Journal of Applied Physics*, vol. 105, pp. 1-9, 2009.
- [78] J. Choi, W. Ahn, S. Bae, D. Lee and Y. Kim, "Adenoviral p53 effects and cell-specific E7 protein-protein interactions of human cervical cancer cells," *Biosensors and Bioelectronics*, vol. 20, pp. 2236-2243, 2005.
- [79] M. L. Ermini, S. Mariani, S. Scarano and M. Minunni, "Direct detection of genomic DNA by surface plasmon resonance imaging: An optimized approach," *Biosensors and Bioelectronics*, no. 40, pp. 193-199, 2012.
- [80] M. Vala, R. Robelek, M. Bockova, J. Wegener and J. Homola, "Real-time label-free monitoring of the cellular response to osmotic stress using conventional and long-range surface plasmons," *Biosensors and Bioelectronics*, no. 40, pp. 417-421, 2012.
- [81] J. Merlein, K. Matthial, A. Zuschlag, A. Sell, A. Halm, J. Boneberg, P. Leiderer, A. Leitenstorfer and R. Bratschitsch, "Nanomechanical Control of an Optical Antenna," *Nature Photonics*, vol. 2, no. 27, pp. 203-233, 2008.
- [82] G. Cao, *Nanostructures & Nanomaterials*, London: Imperial College Press, 2004.
- [83] C. J. Brinker and G. W. Scherer, *Sol-Gel Science*, San Diego: Academic Press, Inc, 1990.
- [84] J. S. Shumaker-Parry and J.-W. Park, "Structural Study of Citrate Layers on Gold Nanoparticles: Role of Intermolecular Interactions in Stabilizing Nanoparticles," *Journal of the American Chemical Society*, vol. 136, pp. 1907-1921, 2014.
- [85] Z. Crljen, P. Laxic, D. Sokcevic and R. Brako, "Relaxation and reconstruction on $\tilde{N} 111 \tilde{O}$ surfaces of Au, Pt, and Cu," *Physical Review*, vol. 68, pp. 1-8, 2003.
- [86] M. Mansfield and R. J. Needs, "Application of the Frenkel-Kontorova model to surface reconstructions," *Journal of Physics: Condensed Matter*, vol. 2, no. 10, pp. 2361-2374, 1990.
- [87] N. A. Alcantar, C. Park, J.-M. Pan and J. N. Israelachvili, "Adhesion and coalescence of ductile metal surfaces and nanoparticles," *Science Direct*, vol. 51, pp. 31-47, 2003.

- [88] E. V. Iski, A. D. Jewell, H. L. Tierney, G. Kyriakou and E. C. Kykes, "Controllable restructuring of a metal substrate: Tuning the surface morphology of gold," *Surface Science*, vol. 606, pp. 536-541, 2012.
- [89] H. B. G. Casimir and D. Polder, "The Influence and Retardation on the London-van der Waals Forces," *Physical Review*, vol. 73, no. 4, pp. 360-372, 1947.
- [90] F. M. Serry, D. Walliser and G. J. Maclay, "The Anharmonic Casimir Oscillator (ACO)-The Casimir Effect in a Model Microelectromechanical System," *Journal of Microelectromechanical Systems*, vol. 4, no. 4, pp. 193-205, 1995.
- [91] S. K. Lamoreaux, "Demonstration of the Casimir Force in the 0.6 to 6 μm Range," *Physical Review Letters*, vol. 78, no. 1, pp. 5-8, 1997.
- [92] J. Zou, Z. Marcet, A. W. Rodriguez, M. T. H. Reid, A. P. McCauley, I. I. Kravchenko, T. Lu, Y. Bao, S. G. Johnson and H. B. Chan, "Casimir forces on a silicon micromechanical chip," *Nature Communications*, vol. 4, no. 1845, pp. 1-6, 2013.
- [93] E. M. Lifshitz, "The Theory of Molecular Attractive Forces between Solids," *Soviet Physics*, vol. 29, pp. 94-110, 1956.
- [94] I. E. Dzyaloshinskii, E. M. Lifshitz and L. P. Pitaevskii, "General Theory of Van der Waals' Forces," *Soviet Physics*, vol. 73, pp. 381-422, 1961.
- [95] J. N. Munday, F. Capasso and V. A. Parsegian, "Measured long-range repulsive Casimir – Lifshitz forces," *Nature Letters*, vol. 457, pp. 170-173, 2009.
- [96] M. Grouchko, P. Roitman, X. Zhu, I. Popov, A. Kamyshny, H. Su and S. Magdassi, "Merging of metal nanoparticles driven by selective wettability of silver nanostructures," *Nature Communications*, vol. 5, pp. 1-5, 2014.
- [97] C. Liu, Y.-J. Li, S.-G. Sun and E. S. Yeung, "Room-temperature cold-welding of gold nanoparticles for enhancing the electrooxidation of carbon monoxide," *Chemical Communications*, vol. 14, pp. 4481-4483, 2011.
- [98] G. S. Ferguson, M. K. Chaudhury, G. B. Sigal and G. M. Whitesides, "Contact Adhesion of Thin Gold Films on Elastomeric Supports: Cold Welding Under Ambient Conditions," *Science*, vol. 253, no. 5021, pp. 776-778, 1991.
- [99] R. Feynman, *The Feynman Lectures*, Redwood City, CA: Addison-Wesley, 1964.

- [100] A. D. McFarland, C. L. Haynes, C. A. Mirkin, R. P. Van Duyne and H. A. Godwin, "Color My Nanoworld," *Journal of Chemical Education*, vol. 81, no. 4, pp. 544A-544B, 2004.
- [101] Ratyakshi and R. P. Chauhan, "Colloidal Synthesis of Silver Nano Particles," *Asian Journal of Chemistry*, vol. 21, no. 10, pp. 113-116, 2009.
- [102] L. Obreja, N. Foca, M. I. Popa and V. Melnig, "Alcoholic Reduction Platinum Nanoparticles Synthesis by Sonochemical Method," *SCIENTIFIC ANNALS OF "ALEXANDRU IOAN CUZA DIN IAȘI" UNIVERSITY*, pp. 31-36, 2008.
- [103] T. Herricks, J. Chen and Y. Xia, "Polyol Synthesis of Platinum Nanoparticles: Control of Morphology with Sodium Nitrate," *Nano Letters*, vol. 4, no. 12, pp. 2367-2371, 2004.
- [104] B. T. Draine and P. J. Flatau, "User Guide for the Discrete Dipole Approximation Code DDSCAT 7.1," 8 February 2010. [Online]. Available: <http://arxiv.org/abs/1002.1505>. [Accessed 21 April 2014].
- [105] B. Draine and P. Flatau, "Discrete-dipole approximation for scattering calculations," *Journal of the Optical Society of America A*, vol. 11, no. 4, pp. 1491-1499, 1994.
- [106] B. K. Juluri, "DDSCAT and electric field at at plasmon resonance," 26 May 2010. [Online]. Available: <http://juluribk.com/2010/05/26/ddscat-and-electric-field-at-plasmon-resonance/>. [Accessed 22 April 2014].
- [107] P. Johnson and R. Christy, "Optical constants of the noble metals," *Physical Review B*, vol. 6, no. 12, pp. 4370-4379, 1972.
- [108] J. A. Stratton, *Electromagnetic Theory*, Wiley - IEEE Press, 2007.
- [109] P. T. Sharp, "Sigma-Aldrich," 2014. [Online]. Available: <http://www.sigmaaldrich.com/technical-documents/articles/biofiles/centrifugation-basics.html>. [Accessed 30 May 2014].
- [110] J. A. Lightfoot, M. H. Rosevear, A. M. O'Donnell, E. C. Platz, A. S. Loening and E. C. Hawtrey, "Rubin H. Flocks and Colloidal Gold Treatments for Prostate Cancer," *The Scientific World Journal*, vol. 11, pp. 1560-1566, August 2011.
- [111] G. Grochola, I. K. Snook and S. P. Russo, "Computational modeling of nanorod growth," *The Journal of Chemical Physics*, no. 127, pp. 194707-1 - 194907-13, 2007.
- [112] S. A. Maier, K. P. Kik, H. A. Atwater, S. Meltzer, E. Harel, B. E. Koel and A. G. Requicha, "Local detection of electromagnetic energy transport below the diffraction limit

in metal nanoparticle plasmon waveguides," *Nature Materials*, vol. 2, pp. 229-232, 2003.

[113] P. M. Tomchuk and D. V. Butenko, "The nanoparticle shape's effect on the light scattering cross-section," *Surface Science*, no. 606, pp. 1892-1989, 2012.

[114] N. Kotagiri, *Stealth Carbon Nanotubes: Strategies to Coat Carbon Nanotubes to Prevent Opsonization and Improve Biodistribution*, Ann Arbor, MI: ProQuest LLC, 2011.

Appendix

1. DDSCAT Parameters

'===== Parameter file for v7.3 ====='

**** Preliminaries ****

'NOTORQ' = CMDTRQ*6 (DOTORQ, NOTORQ) -- either do or skip torque calculations

'PBCGS2' = CMDSOL*6 (PBCGS2, PBCGST, GPBICG, QMRCCG, PETRKP) -- CCG method

'GPFAFT' = CMETHD*6 (GPFAFT, FFTMKL) -- FFT method

'GKDLDR' = CALPHA*6 (GKDLDR, LATTD, FLTRCD) -- DDA method

'NOTBIN' = CBINFLAG (NOTBIN, ORIBIN, ALLBIN) -- binary output?

**** Initial Memory Allocation ****

300 150 150 = dimensioning allowance for target generation

**** Target Geometry and Composition ****

'sphroid_2' = CSHAPE*9 shape directive

150 150 150 150 0 1 = shape parameters 1 - 6

2 = NCOMP = number of dielectric materials

'Au_evap' = file with refractive index 1

'Au_evap' = file with refractive index 1

**** Additional Nearfield calculation? ****

0 = NRFLD (=0 to skip nearfield calc., =1 to calculate nearfield E)

0.0 0.0 0.0 0.0 0.0 0.0 (fract. extens. of calc. vol. in -x,+x,-y,+y,-z,+z)

**** Error Tolerance ****

1.00e-5 = TOL = MAX ALLOWED (NORM OF $|G\rangle = AC|E\rangle - ACA|X\rangle$)/(NORM OF $AC|E\rangle$)

**** Maximum number of iterations ****

1000 = MXITER

**** Integration limiter for PBC calculations ****

1.00e-2 = GAMMA (1e-2 is normal, 3e-3 for greater accuracy)

**** Angular resolution for calculation of <cos>, etc. ****
 0.5 = ETASCA (number of angles is proportional to $[(3+x)/ETASCA]^2$)
 **** Wavelengths (micron) ****
 0.4 0.8 27 'INV' = wavelengths (1st,last,howmany,how=LIN,INV,LOG,TAB)
 **** Refractive index of ambient medium ****
 1.3330 = NAMBIENT
 **** Effective Radii (micron) ****
 0.007 0.007 2 'LIN' = eff. radii (1st,last,howmany,how=LIN,INV,LOG,TAB)
 **** Define Incident Polarizations ****
 (0,0) (1.,0.) (0.,0.) = Polarization state e01 (k along x axis)
 2 = IORTH (=1 to do only pol. state e01; =2 to also do orth. pol. state)
 **** Specify which output files to write ****
 1 = IWRKSC (=0 to suppress, =1 to write ".sca" file for each target orient.
 **** Specify Target Rotations ****
 0. 0. 1 = BETAMI, BETAMX, NBETA (beta=rotation around a1)
 0. 0. 1 = THETMI, THETMX, NTHETA (theta=angle between a1 and k)
 0. 0. 1 = PHIMIN, PHIMAX, NPHI (phi=rotation angle of a1 around k)
 **** Specify first IWAV, IRAD, IORI (normally 0 0 0) ****
 0 0 0 = first IWAV, first IRAD, first IORI (0 0 0 to begin fresh)
 **** Select Elements of S_{ij} Matrix to Print ****
 9 = NSMELTS = number of elements of S_{ij} to print (not more than 9)
 11 12 21 22 31 33 44 34 43 = indices ij of elements to print
 **** Specify Scattered Directions ****
 'TFRAME' = CMDFRM (LFRAME, TFRAME for Lab Frame or Target Frame)
 1 = NPLANES = number of scattering planes
 0. 0. 180. 1 = phi, theta_min, theta_max (deg) for plane A